Lactational delivery of Triclosan promotes non-alcoholic fatty liver disease in newborn mice

André A. Weber[1], Xiaojing Yang[1], Elvira Mennillo[1], Jeffrey Ding[2], Jeramie D. Watrous[2], Mohit Jain[2], Shujuan Chen[1], Michael Karin[3], Robert H. Tukey[1,*].

Short Title: *Triclosan drives neonatal NAFLD*

[1]Laboratory of Environmental Toxicology, Department of Pharmacology, University of California, San Diego, La Jolla, CA 92093, USA.

[2]Departments of Medicine and Pharmacology, University of California, San Diego, La Jolla, CA 92093, USA.

[3]Laboratory of Gene Regulation and Signal Transduction, Department of Pharmacology, University of California, San Diego, La Jolla, CA 92093.

Correspondence should be addressed to Robert H. Tukey. rtukey@health.ucsd.edu: UC San Diego, 9500 Gilman Drive, La Jolla, CA 92093-0722

Conflict of Interest Statement: The authors disclose no additional conflicts.

Keywords: lactation, lipogenesis, endoplasmic reticulum stress, nonalcoholic FLD, nonalcoholic steatohepatitis, toxicant-associated steatohepatitis.

ABBREVIATIONS

ACACA, acetyl-CoA carboxylase 1; ACLY, ATP citrate lyase; AMPK, adenosine monophosphate (AMP)–activated protein kinase; ATF4, Activating transcription Factor 4; CCNE1, cyclin e1; CLDN, Claudin; CTGF, connective tissue growth factor, CYP4A10, cytochrome P450, family 4, subfamily a, polypeptide 10; CYP4A14, cytochrome P450, family 4, subfamily a, polypeptide 14; CYP7A1, Cholesterol 7 alpha-hydroxylase; DNL, de novo lipogenesis; EHHADH, Enoyl-CoA Hydratase and 3-Hydroxyacyl CoA Dehydrogenase; eIF2α, eukaryotic translation initiation factor 2 alpha; ER, endoplasmic reticulum; FABP1, fatty acid binding protein 1; FASN, fatty acid synthase; FGF21, fibroblast growth factor 21; FL, fatty liver; FLD, fatty liver disease; FOXO1, forkhead box O1; FXR, farnesoid X receptor; $gp130^{Act}$, active glycoprotein 130; GR, glucocorticoid receptor; HCC, hepatocellular carcinoma; IB, immunoblotting; IL1β, interleukin 1 beta; LC-MS, Liquid chromatography mass spectrometry; MCM, mini-chromosome maintenance; MLXIPL, MLX-interacting protein-like; NAFLD, non-alcoholic FLD; NASH, non-alcoholic steatohepatitis, NQO-1, NAD(P)H dehydrogenase [quinone] 1; OCA, obeticholic acid; ORO, oil red O; PERK, PKR-like ER kinase; PPARα, peroxisome proliferator-activated receptor alpha, SCD1, stearoyl-CoA desaturase-1; SHP, small heterodimer partner; SREBF1, sterol regulatory element-binding protein 1; TG, triglyceride; TJP, tight junction protein; TCS, triclosan; UPR, unfolded protein response; YAP, yes-associated protein-1; WT, wild-type.

ABSTRACT

Pediatric non-alcoholic fatty liver disease (NAFLD) is escalating in the United States, with a limited mechanistic understanding. Triclosan (TCS) is a high-volume antimicrobial additive that has been detected in human breastmilk and shown in adult mice to cause hepatosteatosis. To examine the effect of TCS presented to neonatal mice through lactation, we exposed pregnant females to TCS in their diet and evaluated its impact on nursing neonates. TCS is efficiently transferred by lactation to newborn mice, causing significant fatty liver (FL) during the suckling period. Lactational delivery stimulated hepatosteatosis, triglyceride accumulation, endoplasmic reticulum (ER) stress, inflammation, and liver fibrosis. These events were mirrored by inhibition of key metabolic regulators, FGF21 and AMPK. De novo lipogenesis (DNL) induced by lactational TCS exposure was blocked in mice deficient in hepatic ATF4 . In primary hepatocytes, siRNA specific inhibition of PERK, an ATF4 upstream activator and initiator of ER stress, blocked TCS induced DNL. Also, in the absence of PPARα, which targets regulation of ATF4, TCS induced triglyceride accumulation and the induction of DNL was blocked. The administration of obeticholic acid (OCA), a potent FXR agonist, as well as activation of intestinal mucosal-regenerative gp130 signaling, led to reduced liver ATF4 expression, PPARα signaling, and DNL when neonates were exposed to TCS. In summary, TCS exposure via lactation leads to early indicators of NAFLD development accompanied by hepatosteatosis that were mediated in a PERK-eIF2α-ATF4-PPARα cascade. These studies indicate that mother to child transmission of environmental toxicants such as TCS may underlie the recent increases in pediatric NAFLD.

INTRODUCTION

Nonalcoholic FLD (NAFLD) has emerged as the most common liver disorder worldwide, paralleling the obesity and diabetes epidemics[1]. The prevalence of NAFLD in adults in Western countries is estimated between 20-30% and approximately 10-20% of these cases have a more severe manifestation named non-alcoholic steatohepatitis (NASH)[2]. Although NASH usually appears in adults, there is an alarming increase in NAFLD in children, termed pediatric NAFLD[3,4], which is a prerequisite towards NASH development. Epidemiological studies have shown a prevalence of pediatric NAFLD in up to 10% of the pediatric population[5]. NAFLD in children displays the same morphological lesions observed in adults, however, the distribution of these lesions is frequently different. For example, in adult's, steatosis starts in the perivenular zone, while in children steatosis starts in the periportal zone[6]. The progression of simple steatosis to NASH depends on multiple parallel hits, including endoplasmic reticulum (ER) stress, inflammation, defective lipid export, enhanced de novo lipogenesis (DNL) and deterioration of the intestinal barrier[7-10].

Physiological changes and different pathological conditions can activate an elaborate signaling pathway called integrated stress response (ISR). Extrinsic (hypoxia, amino acid deprivation and viral infection) and intrinsic (ER) stresses can activate ISR. ER stress, which plays an important role in fatty liver disease (FLD), activates the activating transcription factor 4 (ATF4) through protein kinase R like kinase (PERK)[11]. Peroxisome proliferator-activated receptor α (PPARα) is also a key regulator of hepatic fatty acid oxidation (FAO) and lipid metabolism[12]. However, the involvement of PPARα in the progression of FLD is controversial[13,14]. Moreover, PPARα has a strong link to ER stress signaling. *Atf4*-null mice challenged with a high fructose diet have exhibited diminished lipogenesis and PPARα target gene expression[15]. PPARα also has a strong link with ATF6, another ER sensor. Overexpression of ATF6 in NAFLD livers leads to activation of the ATF6-PPARα axis, promoting an increase in hepatic FAO genes

including fibroblast growth factor 21 (*Fgf21*), a liver-secreted cytokine that regulates hepatic metabolic processes, including fat oxidation, gluconeogenesis, and metabolic gene expression[16]. FGF21 has been shown to ameliorate NAFLD[17].

Environmental toxicants in the absence of caloric overload can induce FLD or toxicant associated FLD (TAFLD)[18,19]. Triclosan (TCS) is a high-volume chemical used as an antimicrobial additive in many human consumer products[20,21]. We have demonstrated that long term TCS exposure in adult mice increased liver-to-body weight (BW) without affecting BW[22]. This resulted in enhanced liver proliferation along with induction of genes linked to fibrogenesis, elevated collagen accumulation, and liver oxidative stress, supporting the notion that TCS may lead to a condition similar to NASH, referred to as toxicant associated steatohepatitis (TASH). We have recently confirmed that TCS induces FLD while blunting HFD-induced expression of FGF21[23].

TCS is a ubiquitous environmental toxicant[21] and has been identified in human breastmilk samples with concentrations up to 2,100 µg/kg of lipids[24,25]. Based upon the volume of breastmilk that an infant consumes per day it has been estimated that a breastfeeding infant can consume 1000-2000 ng of TCS daily[24,26]. In addition, while breastmilk has an important influence on infant survival and health reducing disease risk and promoting aspects of postnatal development[27], environmental toxicants can still be transferred from the nurturing mother to newborns through lactation[28]. The constant presence of TCS in breastmilk in different studies and the high incidence of pediatric NAFLD led us to hypothesize that the transfer of TCS from lactating mothers to newborns can lead to NAFLD in children. To examine the effect of TCS presented to neonatal mice through lactation, we exposed pregnant females to TCS in their diet and evaluated the delivery of TCS through breastmilk. Our findings have confirmed that the delivery of TCS through lactation leads to the precocious development of fatty liver suggesting that exposure of newborns to TCS and other toxicants through lactation maybe a contributing factor to early onset NAFLD and NASH.

RESULTS

TCS stimulates hepatic ER stress and DNL in mice

Mating C57/BL6 mice were placed on a normal chow diet containing 0.012% TCS that was continued after birth with neonates exposed through this route for 21 days. TCS in milk and serum of breastfed neonates was measured by LC-MS/MS analysis. The concentration of TCS in breastmilk isolated from the stomach of neonates was 81 ± 19.5 µg/kg at day 14, while the serum concentration at 21 days of exposure was 52.8 ± 8.5 µg/kg (Fig. 1a). These concentrations were like those reported in milk and serum from human samples[25,29]. Breastfeeding with TCS has no effect on body weight and liver weight (Supplementary Fig. S1a).

Neonatal exposure to TCS through breastmilk resulted in upregulation of ER stress in liver, reflected by induction of the genes glucose-regulated protein 78 (*Grp78*), ER degradation enhancing alpha-mannosidase like protein 1 (*Edem1*), spliced X-box binding protein-1 (*Xbp1s*) and C/EBP homologous protein (*Chop*), with increases in activated phosphorylated eukaryotic translation initiation factor 2α (p-eIF2α) and activating transcription factor 4 (ATF4) (Fig. 1b). Examination of the hepatic gene profile indicated that neonatal mice breastfed with TCS exhibited increased expression of genes that participate in DNL, including sterol regulatory element-binding protein 1 (*Srebf1*), carbohydrate-responsive element-binding protein (ChREBP, encoded by *Mlxipl*), ATP citrate lyase (*Acly*), acetyl-CoA carboxylase (*Acaca*), fatty acid synthase (*Fasn*) and stearoyl-CoA desaturase-1 (*Scd1*) (Fig. 1c). However, there were no statistical differences between vehicle and TCS in expression of fatty acid β-oxidation genes, including peroxisomal acyl-coenzyme A oxidase 1 (*Acox1*) and carnitine palmitoyl transferase I (*Cpt1a*) (Supplementary Fig. 1b). Through immunoblot analysis (IB), FASN, which is a key enzyme in DNL[30], was also increased in livers of TCS breastfed mice (Fig. 1c). Furthermore, the increase in serum alanine aminotransferase (ALT) in TCS exposed mice is an indication that the liver has been damaged (Fig. 1d). By LC-MS/MS, palmitate

in serum of neonates was two-fold higher than in control-fed neonatal mice (Fig. 1e). Congruently, liver and serum triglycerides (TG) were elevated in neonatal mice exposed to TCS (Fig. 1e). Oil Red O (ORO) staining showed accumulation of lipid droplets in the cytoplasm of hepatocytes from TCS treated neonatal mice (Fig. 1f). However, Ki-67 staining and TUNEL assay revealed no effects of TCS on proliferation and cell death, respectively (Supplementary Fig. S1c and d).

TCS stimulates ER stress, DNL and PPARα in primary hepatocytes

To investigate the effects of TCS in vitro, we treated primary hepatocytes with TCS at 30 µM for 72 hours. After treatment, TCS was shown to upregulate genes driving DNL including *Fasn*, *Acaca*, *Mlxipl*, *Acly* and *Srebf1* (Fig. 2a), in addition to PPARα target genes (*Cyp4a10* and *Cyp4a14*) (Fig. 2b). Significant induction was also observed with genes associated with ER stress (*Grp78, Xbp1s* and *Chop*) (Fig. 2c). These findings suggest that a strong correlation exits between TCS exposure and ER stress. Induction of genes linked to ER stress in vivo and in vitro led us to speculate that ER stress may be linked to PERK activation followed by ATF4 activation. To examine this possibility, we first treated primary hepatocytes with PERK specific siRNA. Q-RT-PCR analysis confirmed downregulation of *Perk* gene expression (Fig. 2d). In the absence of PERK specific siRNA, ATF4 was induced by TCS, as shown by IB analysis. However, in the presence of PERK specific siRNA, TCS treatment did not induce ATF4 (Fig. 2e). These findings indicate that PERK activation and induction of ATF4 underlie the processes leading to ER stress and induction of DNL.

TCS induces NAFLD and HCC-related genes

Utilizing RNA-seq analysis to investigate those pathways in neonate liver impacted by lactational TCS delivery, results showed that TCS exposure was associated with alterations in more than 410 upregulated genes and 532 downregulated genes, with

an adjusted *P* value less than 0.05 (Supplementary Fig. S2). Gene ontology profiles revealed that TCS robustly induced genes linked to lipogenesis, fatty acid uptake, cholesterol biosynthesis and acylglycerol metabolism. Another set of genes increased by TCS treatment are the major urinary protein (*Mup*) genes, including, *Mup17*, *Mup19*, *Mup15*, *Mup9* and *Mup3* (Fig. 3a). TCS exposure also increased genes associated with retinol metabolism, including cytochrome P450 26A1 (*Cyp26a1*), dehydrogenase/reductase SDR family member 4 (*Dhrs4*) and 9 (*Dhrs9*), aldehyde dehydrogenase family 1, subfamily A7 (*Aldh1a7*) and patatin-like phospholipase domain-containing protein 3 (*Pnpla3*) (Fig. 3a), which has an important role in NAFLD disease progression[31].

Previous results in our laboratory have demonstrated that long-term TCS exposure can promote hepatocellular carcinoma (HCC)[22]. RNA-seq analysis demonstrated that mini-chromosome maintenance (*Mcm*) genes are upregulated in TCS treated mice, which have been reported in several types of cancer, including HCC[32]. Examination of the MCM genes indicated that TCS exhibited an increase in MCM -2, -4, -5, -6, -7, -8 and -10. Several other genes related to HFD-induced HCC[33] that were statistically upregulated by TCS exposure included Golgi membrane protein 1 (*Golm1*), integrin alpha-6 (*Itga6*) and ephrin A1 (*Efna1*) (Fig. 3a). However, many of genes linked to the onset of HCC related genes were not statistically regulated by TCS treatment (Supplementary Fig. S3).

Progression from NAFLD to NASH is accompanied by fibrosis, inflammation, and oxidative stress[7,8,23,31]. In the present study, fibrogenic, oxidative stress, and inflammatory marker genes were upregulated in TCS exposed neonatal mice (Fig. 3b). The increase in CYP7A1, NQO-1, SCD1 and IL-1β were confirmed by IB analysis (Fig. 3c). Sirius red staining and F4/80 immunohistochemistry showed increases in fibrosis and inflammation in TCS treated neonatal mice (Fig. 3d). A semi-quantitative assessment score according to inflammation, fibrosis, steatosis, and cell death in liver

204 indicates a score of 3 in TCS breastfed mice and 0 for neonatal mice breastfed in the
205 absence of TCS exposure (Supplementary Table S1).
206
207 **TCS blocks hepatic glucocorticoid response**
208 TCS exposure abrogated the response to glucocorticoids in the liver.
209 Glucocorticoids activate the glucocorticoid receptor (GR) and regulate important
210 metabolic pathways in the liver, including gluconeogenesis[34], adenosine
211 monophosphate (AMP)–activated protein kinase (AMPK)[35] and the urea cycle[36]. RNA-
212 seq analysis demonstrated that genes related to gluconeogenesis and the urea cycle
213 were significantly downregulated in livers of TCS breastfed mice. Furthermore, gene and
214 protein analysis showed a decrease in expression of forkhead box O1 (*Foxo1*), an
215 important transcription factor involved in gluconeogenesis[37] (Supplementary Fig. S4a-d).
216 We have previously confirmed that TCS disrupted FGF21 expression[23] . GR can
217 control AMPK target genes via FGF21[35]. Q-RT-PCR and ELISA analysis revealed
218 downregulation of FGF21, in both liver and serum of TCS exposed neonatal mice (Fig.
219 4a). Surprisingly, IB analysis showed decreased levels of phosphorylated AMPK in TCS
220 exposed mice. From RNA-seq analysis, AMPK target genes including peroxisome
221 proliferator-activated receptor γ coactivator 1α (*Ppargc1a*), mitochondrial fission factor
222 (*Mff*), unc-51 like autophagy activating kinase 1 (*Ulk1*) and glycogen Synthase 2 (*Gys2*)
223 were also downregulated (Fig. 4b). Other hepatokines including fetuin B (*Fetub*), retinol
224 binding protein 4 (*Rbp4*), fetuin A (*Ahsg*), selenoprotein P (*Selenop*) and
225 growth/differentiation factor 15 (*Gdf15*) (Supplementary Fig. S4e) were downregulated
226 following TCS exposure.
227
228 **ATF4 controls DNL in TCS exposed mice**
229 Q-RT-PCR and IB analysis confirmed the absence of ATF4 in the liver of $Atf4^{\Delta Hep}$
230 mice (Supplementary Fig. S5a). When we examined expression of genes linked to DNL

in *Atf4*$^{F/F}$ and *Atf4*$^{\Delta Hep}$ mice exposed to lactational TCS, Q-RT-PCR analysis showed that induction of *Srebf1*, *Mlxipl*, *Acaca* and *Fasn* genes, all associated with the development of DNL, were abrogated in *Atf4*$^{\Delta Hep}$ neonatal mice exposed to TCS (Fig. 5a). Consistent with these results, TCS exposed *Atf4*$^{\Delta Hep}$ mice had less TG in their livers compared to *Atf4*$^{F/F}$ mice (Fig. 5b). *Atf4*$^{\Delta Hep}$ mice also expressed less FASN (Fig. 5c) and showed reduced TCS-induced lipid accumulation (Fig. 5d).

ATF4 interacts with many transcription factors[11]. To analyze a possible link between ATF4 and PPARα, we examined PPARα target genes in *Atf4*$^{F/F}$ and *Atf4*$^{\Delta Hep}$ mice treated with TCS. Q-RT-PCR analysis showed decreased expression of *Cyp4a10* and *Cyp4a14* in *Atf4*$^{\Delta Hep}$ mice relative to *Atf4*$^{F/F}$ mice (Supplementary Fig. S5b). Furthermore, blockage of PERK in primary hepatocytes with PERK siRNA followed by TCS treatment demonstrated that when the PERK-ATF4 axis is blocked, PPARα target genes (*Cyp4a10*, *Cyp4a14* and *Fabp1*) and several genes associated with DNL (*Srebf1*, *Fasn*, *Acaca* and *Mlxipl*) are downregulated (Fig. 5e). These findings indicate that PPARα acts downstream of ATF4 to control DNL.

PPARα controls DNL in TCS treated mice

Liver tissues from NASH patients exhibit induction of PPARα and its downstream target genes[33]. RNA-seq analysis confirmed that PPARα signaling was activated in livers of TCS exposed neonatal mice (Supplementary Fig. S6). Examining PPARα target gene expression by Q-RT-PCR we found robust upregulation of downstream genes, including *Cyp4a14*, *Ehhadh* and *Cyp4a10* (Fig. 6a). Induction of hepatic *Cyp4a14* by PPARα has been linked to FLD[15].

In addition, PPARα activation by TCS upregulated genes linked to DNL, such as *Mlxipl*, *Acly*, *Acaca*, *Fasn*, *Srebf1* and *Scd1*, whose induction by TCS was blocked in *Pparα*$^{-/-}$ mice (Fig. 6b). IB analysis confirmed reduced expression of FASN and SCD1 proteins in livers of *Pparα*$^{-/-}$ mice exposed to TCS (Fig. 6c). ELISA showed reduced

accumulation of TG in TCS exposed *Pparα*$^{-/-}$ livers (Fig. 6d). Histological analysis of *Pparα*$^{-/-}$ mice exposed to TCS was comparable with that of *Atf4*$^{\Delta Hep}$ mice in which hepatosteatosis was blocked (Fig. 6e). Combined, these results indicate that PPARα is required for induction of hepatosteatosis in TCS exposed neonatal mice.

Obeticholic acid (OCA) blocks TCS induced DNL

Lactational delivery of TCS to neonatal mice resulted in reduced expression of hepatic FXR target genes (Supplemental Fig. S7a). FXR agonists, including OCA, were developed as potential therapeutics for NAFLD and NASH[38-40]. Neonatal mice nursing on normal milk or TCS tainted breastmilk were treated daily from postnatal day 16 to 20 with oral OCA (100 mg/kg) and tissues collected on postnatal day 21. OCA treatment resulted in robust induction of *Shp*, an FXR target gene in liver and small intestine (Fig. 7a and Supplemental Fig. S7b). FXR activation was reported to enhance expression of intestinal barrier genes, such as claudins and tight-junction proteins (TJPs)[45]. However, our results revealed few changes in intestinal tissue of TCS exposed neonates treated with OCA, other than decreased *Tjp1*, *Cldn1* and *Cldn19* mRNAs (Supplemental Fig. S7c).

OCA administration had a significant impact on liver. Q-RT-PCR analysis demonstrated that OCA reduced expression of genes driving DNL including *Mlxipl*, *Acaca*, *Fasn* and *Scd1* (Fig. 7b). OCA also repressed PPARα target genes, including *Cyp4a10*, *Cyp4a14* and *Fabp1*, but only when mice were exposed to TCS (Fig. 7c). The treatment with OCA increases *Fgf21* gene expression even when mice are exposed to TCS (Fig. 7d). ELISA showed reduced hepatic accumulation of TG in mice treated with OCA along with TCS (Fig. 7e). OCA administration along with TCS decreases *Grp78* and *Xbp1s* (Fig. 7f), while IB analysis showed reduced ATF4 and FASN proteins in OCA treated neonatal mice exposed to TCS (Fig. 7g). Importantly, ORO staining revealed a decrease in lipid accumulation in mice treated with OCA along with TCS (Fig. 7h).

OCA administration also had an impact on the GR and AMPK response. Q-RT-PCR analysis demonstrated that OCA increased expression of metallothionein 2 (*Mt2*) and Sulfotransferase Family 1E Member 1 (*Sult1e1*), important GR target genes, only in the absence of TCS. We can conclude that OCA does not stimulate GR targets in the presence of TCS. However, *Ppargc1a*, a key AMPK target gene, plays an important role in FAO and helps to limit lipid accumulation in the liver[41]. While the *Ppargc1a* gene is downregulated by TCS (Fig. 4), OCA overrides this repression by showing considerable induction in the presence of TCS (Supplemental Fig. S7 d), an event that may contribute towards protecting the liver from TCS induced FLD.

Gp130 signaling blocks TCS-induced DNL

An increase in intestinal barrier permeability is one of the factors underlying the progression of NAFLD[10]. TCS treatment damaged the intestinal barrier, as demonstrated by accelerated apoptosis with increases in cytochrome C and induction of caspase-9 and caspase-3 (Fig. 8a). Apoptosis was mirrored by downregulation of claudin mRNAs (*Cldn1* and *Cldn19*) (Fig. 8b). Moreover, the upregulation of several antimicrobial proteins (AMPs), regenerating islet-derived protein 3 beta and gamma (*Reg3b* and *Reg3g*) and resistin-like beta (*Retnlb*), suggested that TCS is causing stress or microbial translocation in the intestinal mucosa (Supplemental Fig. S8a). Furthermore, TCS administration dramatically increased phosphorylated total β-catenin and its targets LGR5 and SGK1 (Supplemental Fig. S8b). β-catenin is known to promote tumorigenesis via the *Wnt* pathway[42]. However, histological analysis did not present any tumor formation (Supplemental Fig. S8c). With induction of intestinal AMPs, TCS administration is causing significant stress without altering the majority of the claudins and TJPs mRNAs (Supplemental Fig. S8 d,e).

Intestinal damage activates yes-associated protein-1 (YAP) and tafazzin (TAZ) to stimulate barrier repair[43]. Indeed, TCS exposure upregulated YAP target genes,

312 including connective tissue growth factor (*Ctgf*) in small intestine and colon and cyclin e1
313 (*Ccne1*) in small intestine (Fig. 8c). Due to tight-junction loss and apoptosis caused by
314 TCS, we examined the actions of lactational TCS exposure on neonatal IEC-specific
315 *gp130*^{Act} mice which show enhanced intestinal barrier repair and upregulation of TJP and
316 claudins[10]. Q-RT-PCR analysis showed that *gp130*^{Act} mice were resistant to TCS-
317 induced *Fasn*, *Scd1*, *Acaca*, *Acly* and *Mlxipl* mRNAs, all of which play important roles in
318 DNL (Fig. 8d). In addition, PPARα target mRNAs, including *Cyp4a10* and *Fabp1* were
319 reduced in livers of TCS exposed *gp130*^{Act} mice (Fig.8e). Hepatic TG levels in g*p130*^{Act}
320 mice treated were also reduced when compared to WT treated mice (Fig. 8f). In addition,
321 mRNA levels of *Grp78* were lower in livers of *gp130*^{Act} mice when compared to WT
322 treated with TCS (Fig. 8g). IB analysis showed lower protein levels of ATF4, FASN and
323 SCD-1 in g*p130*^{Act} mice compared with WT mice both treated with TCS (Fig. 8h).
324 Importantly, ORO staining analysis showed no accumulation of lipid droplets in vehicle
325 and TCS exposed g*p130*^{Act} mice when compared to WT mice exposed to TCS (Fig. 8i).
326 Clearly, g*p130*^{Act} mice are resistant to the early actions of lactational TCS delivery on the
327 development of FL, clearly demonstrating that TCS impacts intestinal barrier integrity.
328

DISCUSSION

TCS, a ubiquitous environmental toxicant that has been detected in urine, blood, and breast milk in different regions of the world suggests that the general population is exposed to TCS[25,44-46]. With considerable evidence that TCS alters biological responses[21], several key studies in mice have confirmed that long term exposure has detrimental effects on both the intestinal tract and liver. Chronic exposure to TCS has been shown to increase colonic inflammation and colitis-associated colon tumorgenesis[47], which has recently been linked to reactivation of TCS from its glucuronide metabolite by specific intestinal microbial β-glucuronidase enzymes[48]. Our previous studies have shown TCS can function as a liver tumor promoter stimulating liver tumorigenesis, due in part to induction of oxidative stress and fibrosis[21,22]. In both a normal chow diet and high fat diet (HFD), TCS increased lipid droplet accumulation in liver[23]. As an adaptive response to HFD and nutrient sensing, the liver-secreted cytokine FGF21 is significantly induced. However, an HFD+TCS greatly blunts expression of FGF21[23], leading us to hypothesize that FGF21 plays an important role in suppressing FL. When we induced a type-1 diabetic animal model by treating newborn mice with streptozotocin to damage insulin-secreting beta cells in the pancreas[49] followed by a HFD, adult mice robustly developed NASH that was significantly accelerated in the presence of TCS[23]. TCS-treated mice exhibited elevated levels of oxidative stress, hepatic fibrosis, and inflammatory responses. With current epidemiological studies convincingly showing the accumulation of TCS in human breast milk, if it is transferred to nursing newborns the dietary conditions would simulate an early dietary based HFD contaminated with TCS. Thus, we developed an animal model that allowed us to examine the impact of lactational TCS delivery to neonates and its potential impact on FLD.

Neonatal mice receiving TCS through lactation exhibit early onset hepatic ER stress and steatosis, two important events that stimulate progression from NAFLD to

NASH[7]. Several mechanisms can lead to the induction of DNL in liver ER stress, including caspase-2 activation[50], inflammation[10], interleukin-17A[51] and the PERK-eIF2α-ATF4 axis[52]. Our findings indicate that ATF4 and PPARα are critical mediators of this process. Ablation of ATF4 or blockage with PERK siRNA prevents DNL related gene induction in neonatal mice receiving TCS through lactation. Interestingly, deletion of PPARα also prevented lipid accumulation in the liver. We had previously shown that PPARα is activated by TCS through an indirect mechanism, as TCS had no effect on PPARα in vitro[22]. Similar outcomes regarding gene expression, TG accumulation and protein expression in both ATF4 and PPARα deficient mice suggest that activation of PPARα depends on ER stress through the PERK-eIF2α-ATF4 pathway.

Due to the role PPARα has on FAO, this nuclear receptor has been extensively studied as a potential target to treat NAFLD[53]. However, we have shown that PPARα ablation is protective in TCS-induced FLD. Furthermore, *Fgf21*, which is a PPARα target gene and plays an important role in fat oxidation[53] is downregulated by TCS treatment, unlike what is seen in HFD fed mice[23]. Polychlorinated biphenyls (PCBs) have been shown to also reduce hepatic *Fgf21* mRNA[19]. Since TCS and other environmental toxicants can reduce FGF21 expression, NAFLD caused by environmental toxicants can be more aggressive than the development of NAFLD caused by HFD. However, the exact mechanism by which TCS downregulates FGF21 remains obscure.

OCA has been tested as a treatment option for several liver diseases including NAFLD and type-2 diabetes[40]. However, there is limited mechanistic understanding of how OCA acts. Our findings demonstrated that the oral administration of OCA dramatically reduces ATF4, PPARα signaling, and several genes associated with DNL in mice exposed to TCS. In addition, activation of gp130 signaling, using the *gp130*^{Act} mouse model, prevented hepatic DNL and ER stress in TCS exposed mice. It is understood that gp130 reduces endotoxemia and decreases liver inflammation, thus decreasing fatty liver progression[10].

In summary, the transmission of TCS through lactation leads to lipogenesis, ER stress, PPARα activation and inflammation in neonatal livers. These events are important for early onset FLD. Mechanistically, both ATF4 and PPARα have an important role in DNL and NAFLD progression. The similarity in function between these two transcription factors suggests they may communicate physically. Further studies are necessary to elucidate this pathway. Administration of OCA and activation of mucosal-regenerative gp130 signaling ameliorates TCS induced FLD, decreasing ER stress, PPARα signaling and DNL. As a ubiquitous environmental toxicant that has been detected in tissues from individuals of all ages[21], TCS may initiate TASH in children. In addition, with the increase in pediatric NAFLD and NASH[3,4], we can suggest that TCS exposure through lactation heightens the sensitivity toward FLD as children are continually exposed to high caloric and energy rich foods.

Acknowledgments. This work was supported by National Institute of Environmental Health Sciences Grants R21-ES031849 (R.H.T.), P42-ES010337 (R.H.T., M.J. and M.K.), R21-AI35677 (S.C.), and a Seed grant to R.H.T. made available through the UC San Diego Larsson-Rosenquist Foundation Mother-Milk-Infant Center of Research Excellence (MOMI CORE). The support of the Family Larsson-Rosenquist Foundation is gratefully acknowledged."

Author contributions

Andre A. Weber. (Conceptualization, Data curation, Data analysis, Writing)

Xiaojing Yang (Data curation)

Elvira Mennillo (Data curation)

Jeffrey Ding (Data curation)

Jeramie D. Watrous (Data curation)

Mohit Jain (Conceptualization, Data analysis, Resources, Funding)

Michael Karin (Conceptualization, Resources, Writing)

Shujuan Chen (Data analysis, Resources)

Robert H. Tukey (Lead, Funding, Supervision, Writing)

FIGURE LEGENDS

Figure 1. Triclosan exposure induces ER stress, stimulates DNL and causes TG accumulation. WT mice breastfed with TCS or vehicle for 14 or 21 days. **a.** TCS was measured in milk from stomach contents of 14-day old mice (n=4-6 per group) and serum at 21 days (n=4 per group). **b.** Expression of hepatic ER stress genes (n=5 per group) and immunoblot (IB) analysis of total and phosphorylated eIF2α and ATF4 in liver lysate from 21-day old mice (n=3 mice per group). **c.** Expression of hepatic lipogenic genes at 21 days (n=6 mice per group) and IB analysis of FASN in livers (n=3 mice per group). **d.** Measurement of ALT in serum at 21-days-old (n=3-5 per group) **e.** Measurement of serum palmitate (%), serum and liver triglycerides (TG) at 21 days (n=3-7 mice per group). **f.** Histology liver sections were stained with H&E and ORO (n=4 per group), Scale bars=20μm. **a**, **b**, **c**, **d** and **e** show mean ± S.E., determined by two-tailed Student`s test; **P*<0.05, ***P*<0.01, ****P*<0.001.

Figure 2. TCS stimulates DNL, ER stress and PPARα in mouse primary hepatocytes and ATF4 induction is PERK dependent. Mouse primary hepatocytes were isolated from one month old mice and were placed in medium with DMSO or in the presence of 30μM of TCS. After 72 hours of exposure the hepatocytes were collected for Q-RT-PCR analysis (n=4 samples per group). **a.** TCS stimulates genes associated with DNL. **b.** Induction of genes associated with ER stress. **c.** downstream PPARα target genes. **d.** hepatocytes were isolated, and cells were transfected with mouse PERK siRNA and control siRNA. Twenty-four hours later, TCS at 30μM was added in the medium and 48-hours later cells were harvested. Q-RT-PCR analysis of *Perk* after treatment with siRNA (n=4 samples per group). **e.** Representative IB analysis were performed for ATF4. **a**, **b**, **c,** and **d** show mean ± S.E., determined by two-tailed Student`s test; **P*<0.05, ***P*<0.01, ****P*<0.001.

Figure 3. TCS induces genes related to NASH and HCC in liver. WT mice breastfed with TCS or vehicle for 21 days. **a.** Heatmaps showing differential expression of genes related to lipogenesis, retinol metabolism and MCM and HCC in 21-day old mice (n=3 per group). **b.** Expression of genes associated with inflammation, fibrotic and oxidative stress (n=3 per group). **c.** Representative IB analysis of NQO1, SCD1 and IL-1β at 21 days. **d.** Histological slides were stained with Sirius Red and F4/80 antibody in liver sections from TCS breastfed (21-day old) or vehicle breast fed WT mice (n=4 per group). **b** and **d** show mean ± S.E., determined by two-tailed Student`s test; **P*<0.05, ***P*<0.01, ****P*<0.001. All genes used are significant and p adjusted value below the cut-off level of 0.05.

Figure 4. TCS blocks *Fgf21* expression and AMPK signaling. WT mice breastfed with TCS or vehicle for 21 days. **a.** Hepatic expression of *Fgf21* was measured by Q-RT-PCR and FGF21 serum levels were evaluated by ELISA in 21-day old mice (n=4 per group). **b.** IB analysis of total and phosphorylated AMPK and expression of AMPK target genes from TCS and WT mice in liver of 21-day old neonatal mice (n=3 per group). **a** and **b** show mean ± S.E., determined by two-tailed Student`s test; **P*<0.05, ***P*<0.01.

Figure 5. ATF4 controls DNL in liver of TCS treated mice. $Atf4^{F/F}$ and $Atf4^{\Delta Hep}$ mice breastfed with vehicle or through lactational delivery of TCS for 21 days. **a.** Expression of hepatic lipogenic genes (n=6 mice per group). **b.** Measurement of liver triglycerides (TG) (n=4-6 mice per group). **c.** IB analysis of FASN in liver lysate from 21-day old mice. **d.** Frozen liver sections were stained with ORO (n=3 per group). Scale bars, 20μm. **E.** Expression of target genes regulated by PPARα and those that participate in DNL following PERK siRNA and TCS treatment (n=4 mice per group). **a** though **e** show mean ± S.E., determined by two-tailed Student`s test; **P*<0.05, ***P*<0.01.

Figure 6. PPARα controls DNL in liver of mice exposed to lactational TCS. WT and *Pparα*$^{-/-}$ neonatal mice breastfed with vehicle or TCS for 21 days. **a.** Expression of PPARα target genes at 21 days (n=6 mice per group). **b.** Expression of genes linked to hepatic lipogenesis (n=4 mice per group). **c.** Hepatic IB analysis of FASN and SCD1. **d.** Measurement of liver triglycerides (TG) at 21 days (n=4 mice per group). **e.** Frozen liver sections were stained with ORO (n=3 per group). Scale bar, 20μm. a, b, e, f, g and i show mean ± S.E., determined by two-tailed Student`s test; **P*<0.05, ***P*<0.01, ****P*<0.001.

Figure 7. Orally administration of OCA suppresses DNL genes, PPARα activity and ER stress in liver of TCS breastfed mice. Neonatal mice receiving a normal diet or TCS through lactation for 21 days. During the course of this exposure, 16-day old mice were treated with OCA for 4 days and tissues collected on day 21. **a.** Expression of hepatic *Shp*. **b.** Expression of genes associated with lipogenesis. **c**. Hepatic expression of PPARα target genes. **d.** Hepatic expression of *Fgf21*. **e.** Measurement of liver TG. **f.** Genes linked to ER stress. **a-f**, (n=4) per group. **g**. Hepatic IB analysis of ATF4 and FASN. **h**. Frozen liver sections were stained with ORO (n=3 per group). Scale bar, 20μm. **a**, **b**, **c**, **d**, **e,** and **f** show mean ± S.E., determined by two-tailed Student`s test; **P*<0.05, ***P*<0.01, ****P*<0.001.

Figure 8. Activation of gp130 suppresses liver DNL, PPARα activity and ER stress in liver of TCS breastfed mice. *gp130*^{Act} mice received normal milk or TCS through lactation for 21 days. **a.** IB analysis of cytochrome C, caspase 9, cleaved caspase-3. **b**, Expression of claudins and IB of claudin-1 in intestines. **c.** Expression of YAP/TAZ target genes in the intestines. **d.** Expression of hepatic lipogenic genes (n=4 mice per group). **e.** Expression of hepatic PPARα target genes. **f**. Measurement of liver TG. **g**. Hepatic genes linked to ER stress. **b-g** used n=4 mice per group. **h.** Representative IB analysis

of ATF4, FASN and SCD1.**i**, Frozen liver sections were stained with ORO (n=3 per group). Scale bar, 20μm. b-g and f show mean ± S.E., determined by two-tailed Student`s test; **P*<0.05, ***P*<0.01, ****P*<0.001.

Figures

Figure 1

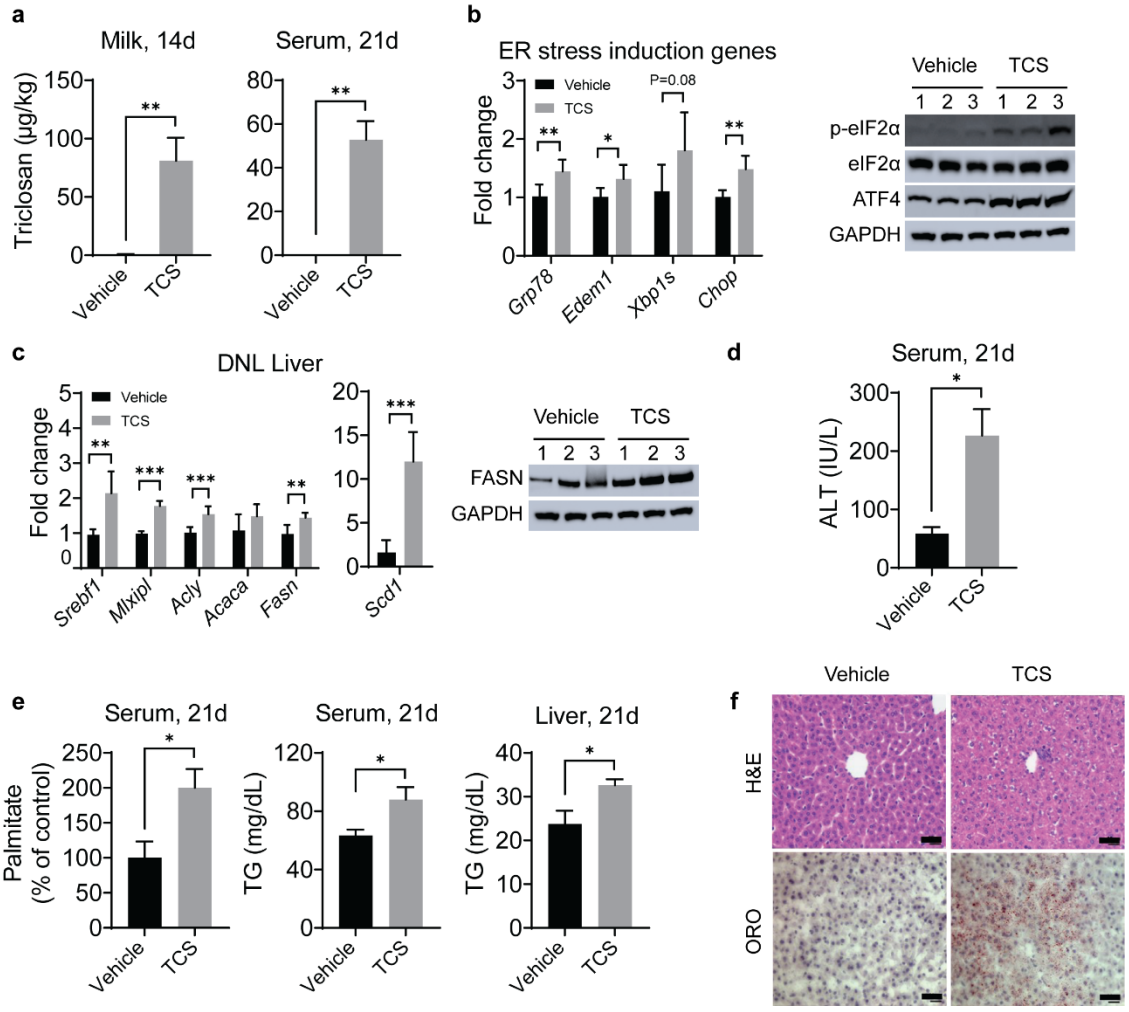

512 **Figure 2**

513

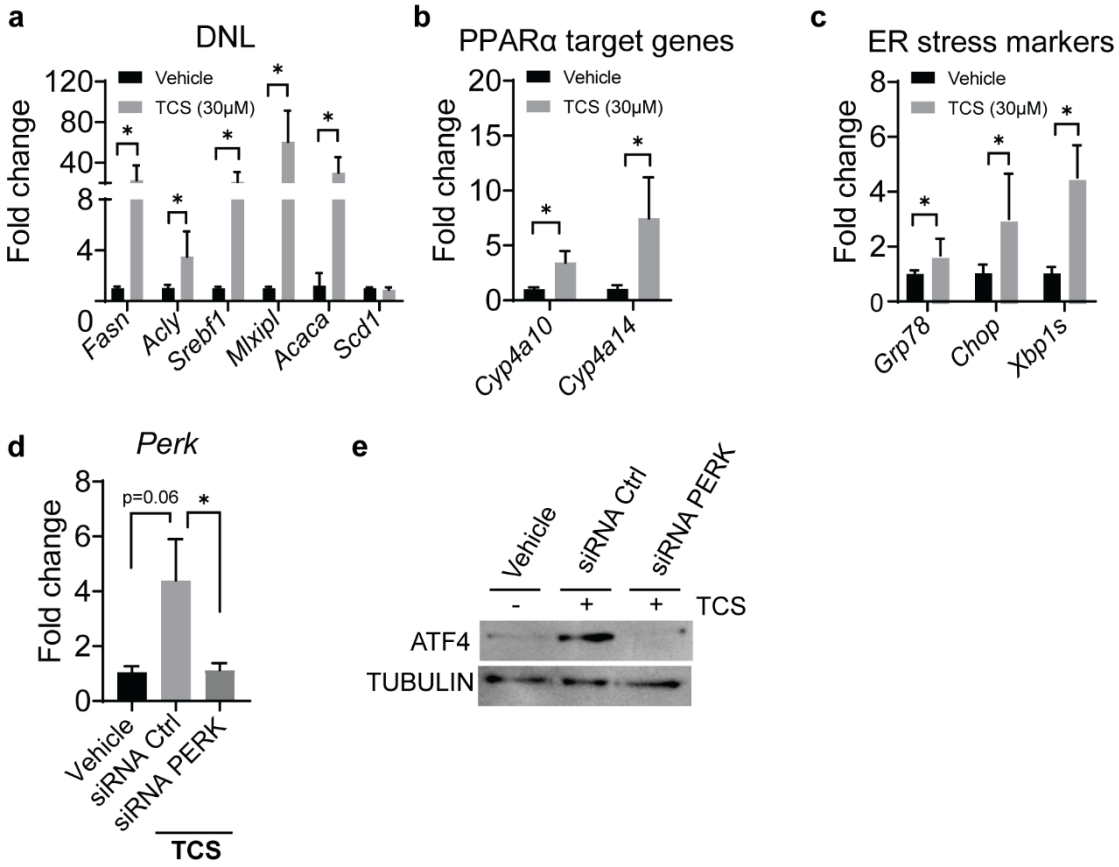

514

515

516 **Figure 3**

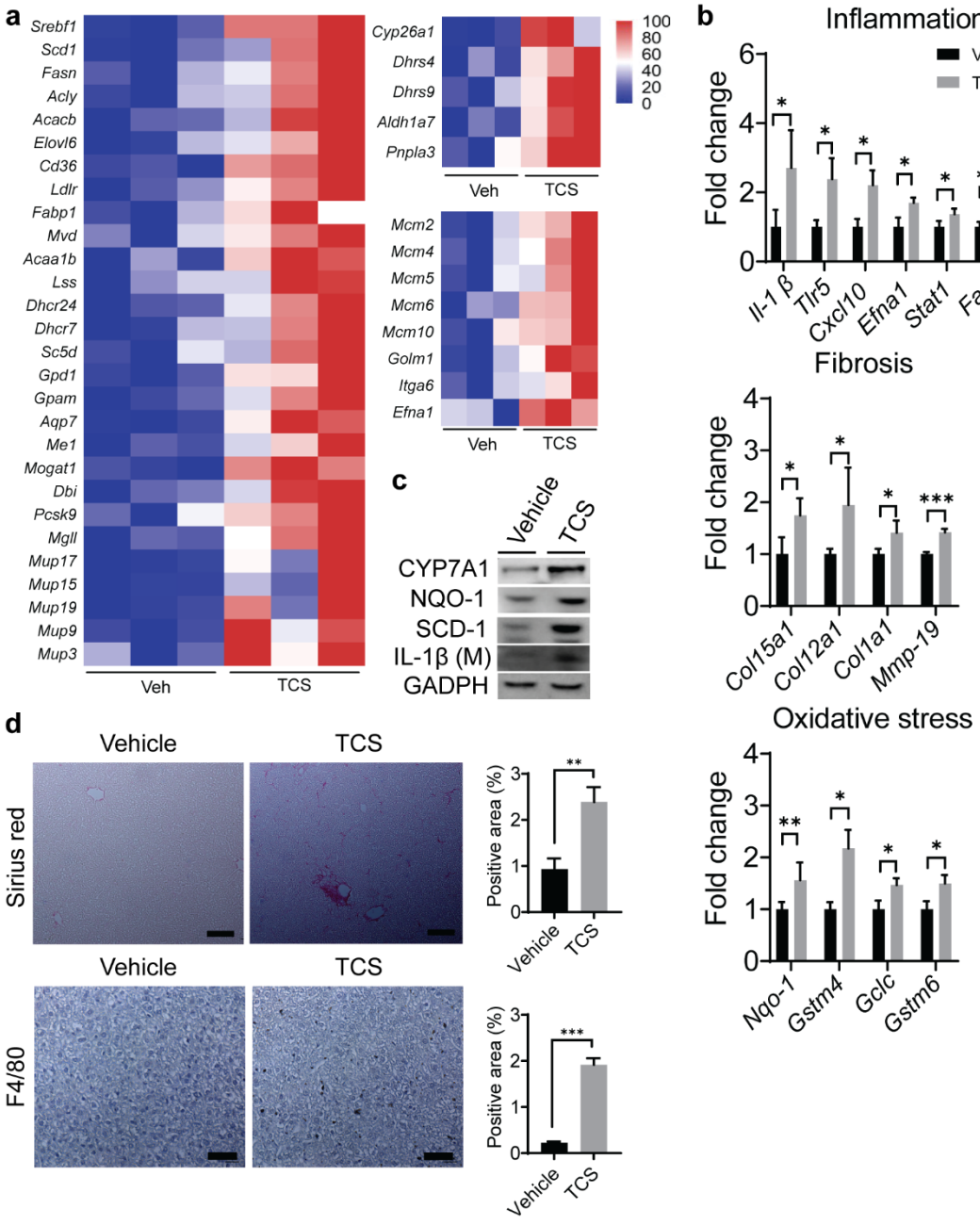

517

518

519 **Figure 4**

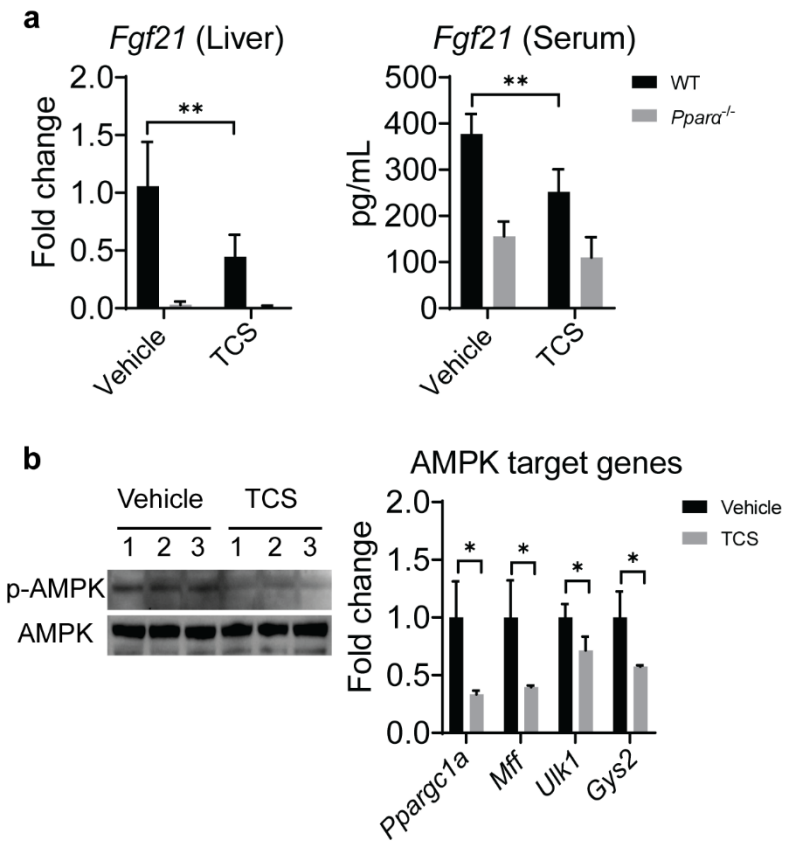

520

521

522 **Figure 5**

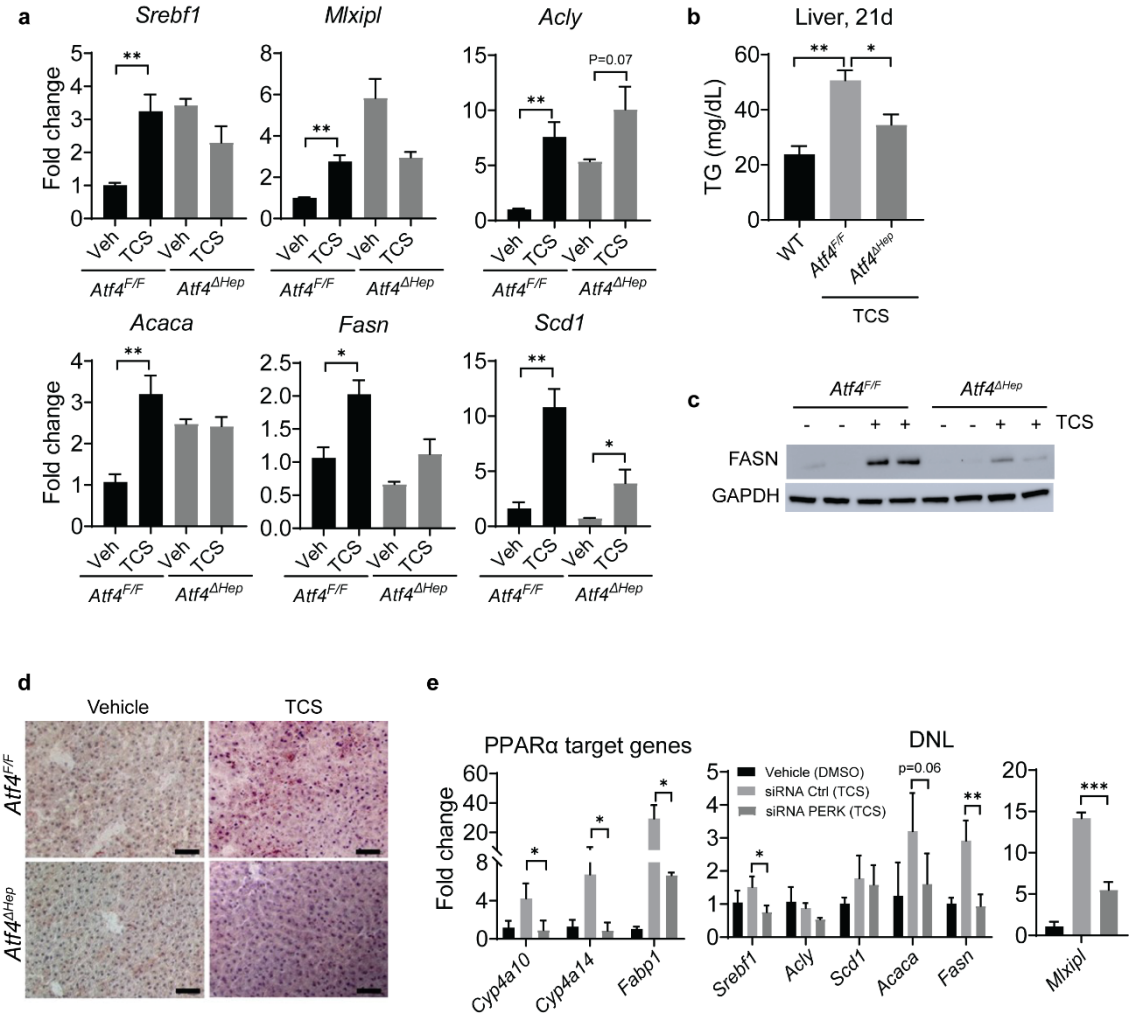

523

524

525 **Figure 6**

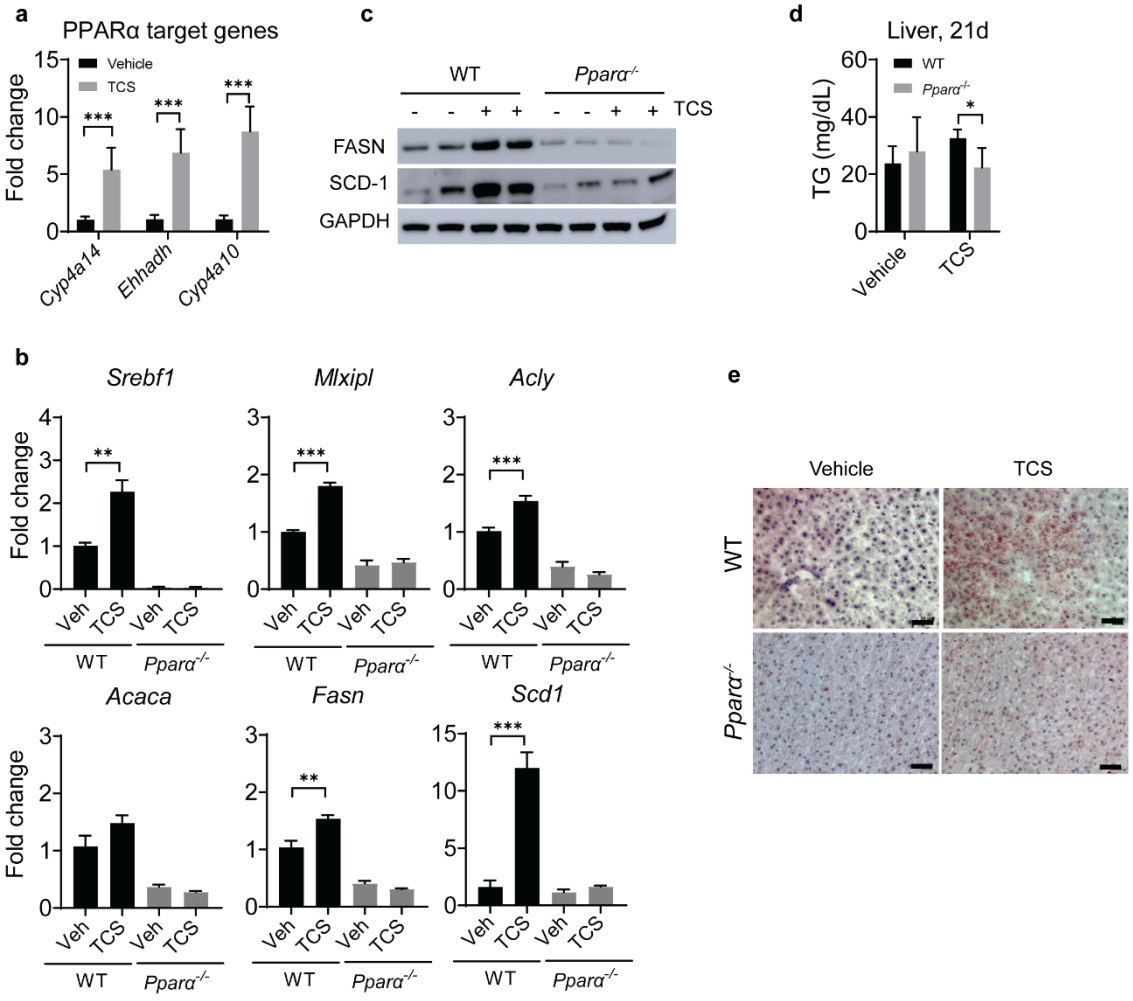

526

527

528 **Figure 7**

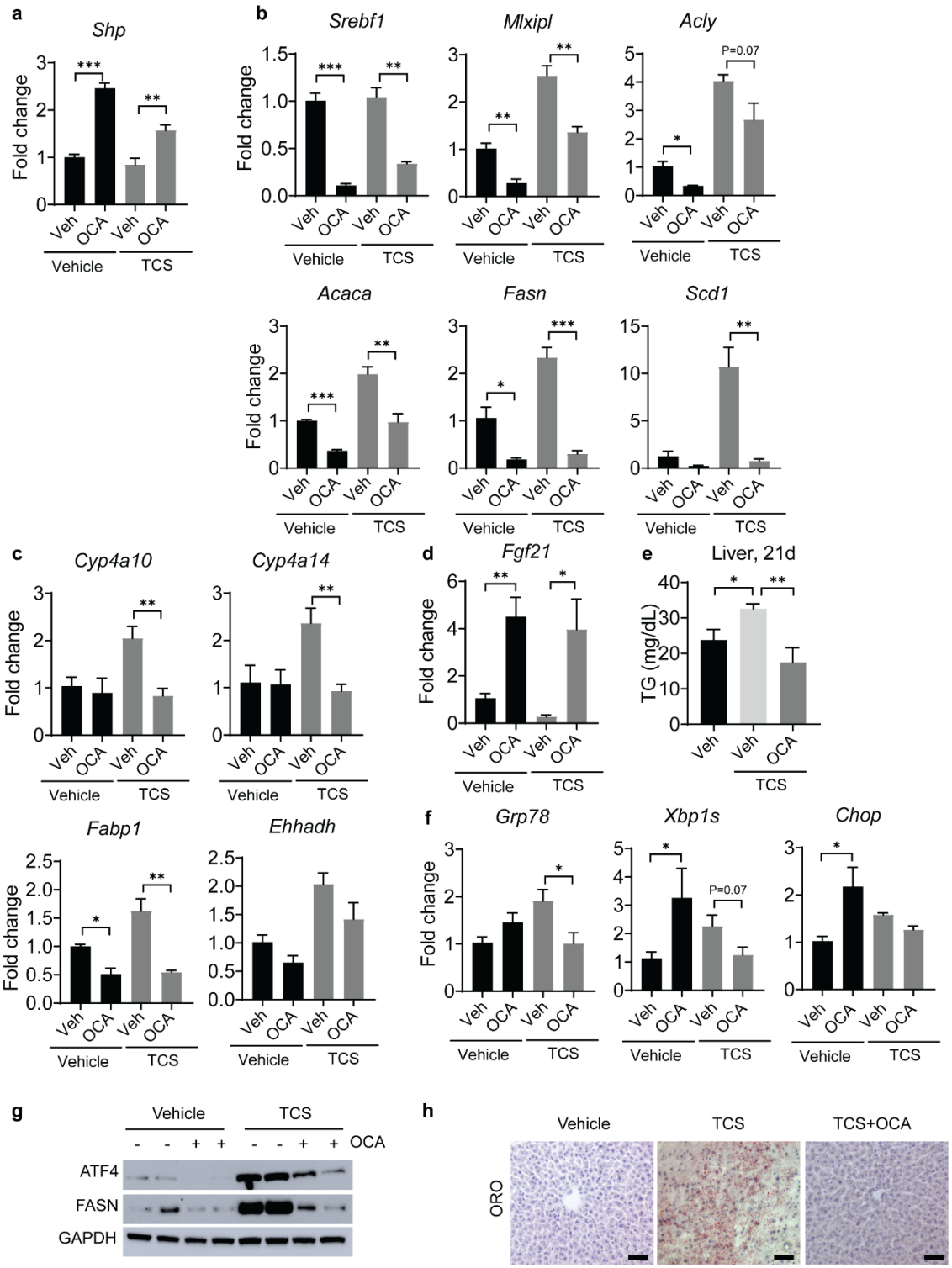

529

530

Figure 8

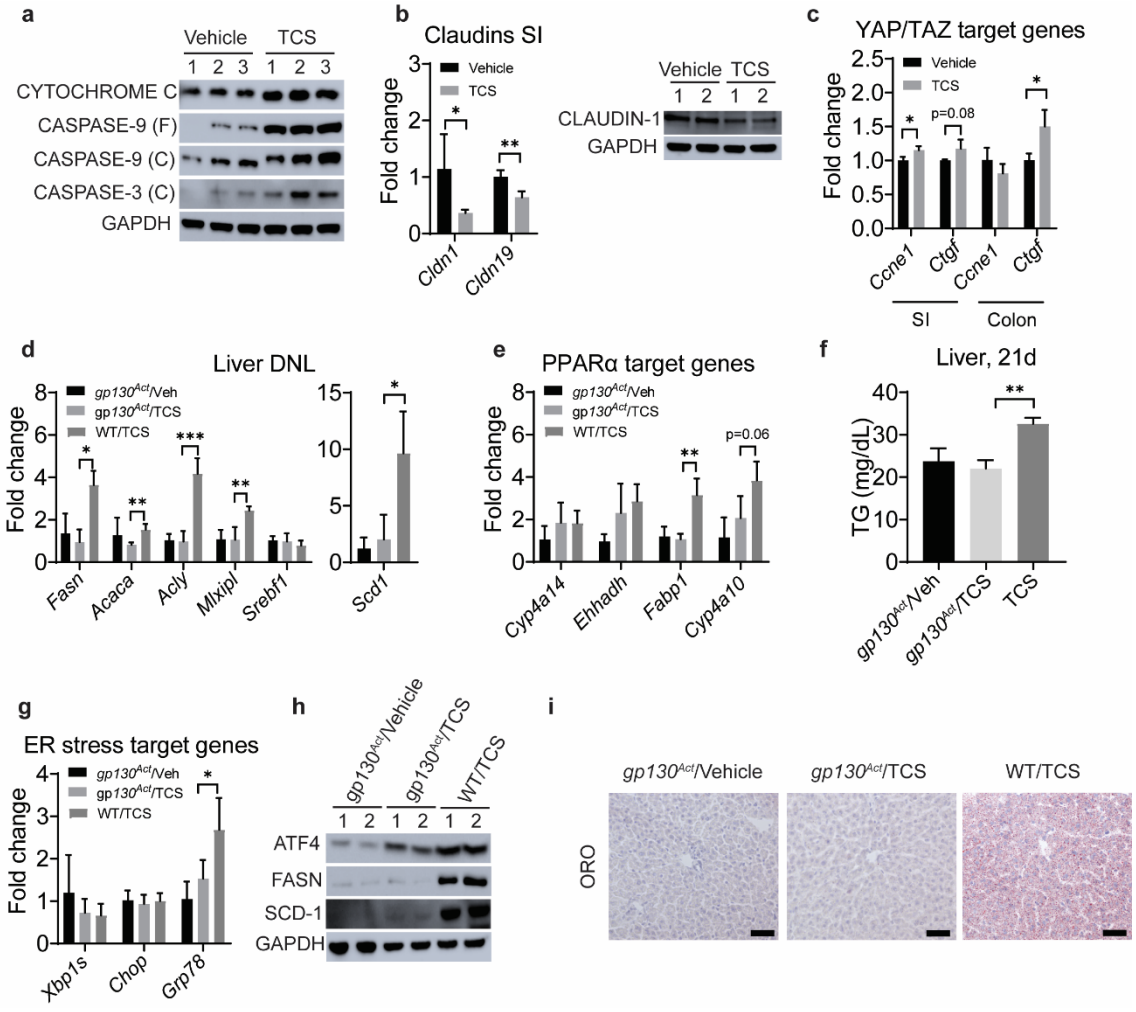

References

1. Spengler, E.K. & Loomba, R. Recommendations for Diagnosis, Referral for Liver Biopsy, and Treatment of Nonalcoholic Fatty Liver Disease and Nonalcoholic Steatohepatitis. *Mayo Clin Proc* **90**, 1233-1246 (2015).
2. Masarone, M., Federico, A., Abenavoli, L., Loguercio, C. & Persico, M. Non alcoholic fatty liver: epidemiology and natural history. *Rev Recent Clin Trials* **9**, 126-133 (2014).
3. Kohli, R.*, et al.* Pediatric Nonalcoholic Fatty Liver Disease: A Report from the Expert Committee on Nonalcoholic Fatty Liver Disease (ECON). *J. Pediatr* (2016).
4. Goyal, N.P. & Schwimmer, J.B. The Progression and Natural History of Pediatric Nonalcoholic Fatty Liver Disease. *Clin Liver Dis* **20**, 325-338 (2016).
5. Schwimmer, J.B.*, et al.* Prevalence of fatty liver in children and adolescents. *Pediatrics* **118**, 1388-1393 (2006).
6. Alisi, A., Feldstein, A.E., Villani, A., Raponi, M. & Nobili, V. Pediatric nonalcoholic fatty liver disease: a multidisciplinary approach. *Nat Rev Gastroenterol Hepatol* **9**, 152-161 (2012).
7. Tilg, H. & Moschen, A.R. Evolution of inflammation in nonalcoholic fatty liver disease: The multiple parallel hits hypothesis. *Hepatology* **52**, 1836-1846 (2010).
8. Lebeaupin, C.*, et al.* Endoplasmic reticulum stress signalling and the pathogenesis of non-alcoholic fatty liver disease. *J Hepatol* **69**, 927-947 (2018).
9. Rahman, K.*, et al.* Loss of Junctional Adhesion Molecule A Promotes Severe Steatohepatitis in Mice on a Diet High in Saturated Fat, Fructose, and Cholesterol. *Gastroenterology* **151**, 733-746.e712 (2016).
10. Todoric, J.*, et al.* Fructose stimulated de novo lipogenesis is promoted by inflammation. *Nat Metab* **2**, 1034-1045 (2020).

11. Pakos-Zebrucka, K.*, et al.* The integrated stress response. *EMBO Rep* **17**, 1374-1395 (2016).

12. Evans, R.M. & Mangelsdorf, D.J. Nuclear Receptors, RXR, and the Big Bang. *Cell* **157**, 255-266 (2014).

13. Montagner, A.*, et al.* Liver PPARalpha is crucial for whole-body fatty acid homeostasis and is protective against NAFLD. *Gut* **65**, 1202-1214 (2016).

14. Zhang, X.*, et al.* Ablation of cytochrome P450 omega-hydroxylase 4A14 gene attenuates hepatic steatosis and fibrosis. *Proc Natl Acad Sci U S A* **114**, 3181-3185 (2017).

15. Xiao, G.*, et al.* ATF4 protein deficiency protects against high fructose-induced hypertriglyceridemia in mice. *J Biol Chem* **288**, 25350-25361 (2013).

16. Fisher, F.M. & Maratos-Flier, E. Understanding the Physiology of FGF21. *Annu Rev Physiol* **78**, 223-241 (2016).

17. Chen, X.*, et al.* Hepatic ATF6 Increases Fatty Acid Oxidation to Attenuate Hepatic Steatosis in Mice Through Peroxisome Proliferator-Activated Receptor α. *Diabetes* **65**, 1904-1915 (2016).

18. Marmugi, A.*, et al.* Low doses of bisphenol A induce gene expression related to lipid synthesis and trigger triglyceride accumulation in adult mouse liver. *Hepatology* **55**, 395-407 (2012).

19. Shi, H.*, et al.* Polychlorinated biphenyl exposures differentially regulate hepatic metabolism and pancreatic function: Implications for nonalcoholic steatohepatitis and diabetes. *Toxicol Appl Pharmacol* **363**, 22-33 (2019).

20. Halden, R.U. On the need and speed of regulating triclosan and triclocarban in the United States. *Environ Sci Technol* **48**, 3603-3611 (2014).

21. Yueh, M.F. & Tukey, R.H. Triclosan: A Widespread Environmental Toxicant with Many Biological Effects. *Annu. Rev. Pharmacol. Toxicol* **56**, 251-272 (2016).

587 22. Yueh, M.F.*, et al.* The commonly used antimicrobial additive triclosan is a liver
588 tumor promoter. *Proc. Natl. Acad. Sci. U. S. A* **111**, 17200-17205 (2014).
589 23. Yueh, M.F.*, et al.* Triclosan leads to dysregulation of the metabolic regulator
590 FGF21 exacerbating high fat diet-induced nonalcoholic fatty liver disease. *Proc*
591 *Natl Acad Sci U S A* (2020).
592 24. Toms, L.M.*, et al.* Triclosan in individual human milk samples from Australia.
593 *Chemosphere* **85**, 1682-1686 (2011).
594 25. Dayan, A.D. Risk assessment of triclosan [Irgasan] in human breast milk. *Food*
595 *Chem. Toxicol* **45**, 125-129 (2007).
596 26. Rodricks, J.V., Swenberg, J.A., Borzelleca, J.F., Maronpot, R.R. & Shipp, A.M.
597 Triclosan: a critical review of the experimental data and development of margins
598 of safety for consumer products. *Crit Rev Toxicol* **40**, 422-484 (2010).
599 27. Victora, C.G.*, et al.* Breastfeeding in the 21st century: epidemiology,
600 mechanisms, and lifelong effect. *Lancet* **387**, 475-490 (2016).
601 28. Allmyr, M., Adolfsson-Erici, M., McLachlan, M.S. & Sandborgh-Englund, G.
602 Triclosan in plasma and milk from Swedish nursing mothers and their exposure
603 via personal care products. *Sci. Total Environ* **372**, 87-93 (2006).
604 29. Sandborgh-Englund, G., Adolfsson-Erici, M., Odham, G. & Ekstrand, J.
605 Pharmacokinetics of triclosan following oral ingestion in humans. *J. Toxicol.*
606 *Environ. Health A* **69**, 1861-1873 (2006).
607 30. Softic, S.*, et al.* Divergent effects of glucose and fructose on hepatic lipogenesis
608 and insulin signaling. *J Clin Invest* **128**, 1199 (2018).
609 31. Saeed, A.*, et al.* Impaired Hepatic Vitamin A Metabolism in NAFLD Mice Leading
610 to Vitamin A Accumulation in Hepatocytes. *Cell Mol Gastroenterol Hepatol* **11**,
611 309-325.e303 (2021).

612 32. Liu, Z., *et al.* MCM family in HCC: MCM6 indicates adverse tumor features and
613 poor outcomes and promotes S/G2 cell cycle progression. *BMC Cancer* **18**, 200
614 (2018).
615 33. Shalapour, S., *et al.* Inflammation-induced IgA+ cells dismantle anti-liver cancer
616 immunity. *Nature* **551**, 340-345 (2017).
617 34. Kuo, T., McQueen, A., Chen, T.C. & Wang, J.C. Regulation of Glucose
618 Homeostasis by Glucocorticoids. *Advances in experimental medicine and biology*
619 **872**, 99-126 (2015).
620 35. Salminen, A., Kauppinen, A. & Kaarniranta, K. FGF21 activates AMPK signaling:
621 impact on metabolic regulation and the aging process. *Journal of molecular*
622 *medicine (Berlin, Germany)* **95**, 123-131 (2017).
623 36. Okun, J.G., *et al.* Molecular regulation of urea cycle function by the liver
624 glucocorticoid receptor. *Molecular metabolism* **4**, 732-740 (2015).
625 37. Puigserver, P., *et al.* Insulin-regulated hepatic gluconeogenesis through FOXO1-
626 PGC-1alpha interaction. *Nature* **423**, 550-555 (2003).
627 38. Nakagawa, H., *et al.* ER stress cooperates with hypernutrition to trigger TNF-
628 dependent spontaneous HCC development. *Cancer Cell* **26**, 331-343 (2014).
629 39. Fang, S., *et al.* Intestinal FXR agonism promotes adipose tissue browning and
630 reduces obesity and insulin resistance. *Nat. Med* **21**, 159-165 (2015).
631 40. Mudaliar, S., *et al.* Efficacy and safety of the farnesoid X receptor agonist
632 obeticholic acid in patients with type 2 diabetes and nonalcoholic fatty liver
633 disease. *Gastroenterology* **145**, 574-582.e571 (2013).
634 41. Piccinin, E., Villani, G. & Moschetta, A. Metabolic aspects in NAFLD, NASH and
635 hepatocellular carcinoma: the role of PGC1 coactivators. *Nat Rev Gastroenterol*
636 *Hepatol* **16**, 160-174 (2019).
637 42. Wang, K., *et al.* SGK1-dependent intestinal tumor growth in APC-deficient mice.
638 *Cell Physiol Biochem* **25**, 271-278 (2010).

639 43. Low, B.C., *et al.* YAP/TAZ as mechanosensors and mechanotransducers in
640 regulating organ size and tumor growth. *FEBS Lett* **588**, 2663-2670 (2014).
641 44. Calafat, A.M., Ye, X., Wong, L.Y., Reidy, J.A. & Needham, L.L. Urinary
642 concentrations of triclosan in the U.S. population: 2003-2004. *Environ. Health*
643 *Perspect* **116**, 303-307 (2008).
644 45. Etzel, T.M., *et al.* Urinary triclosan concentrations during pregnancy and birth
645 outcomes. *Environmental research* **156**, 505-511 (2017).
646 46. Arbuckle, T.E., *et al.* Exposure to free and conjugated forms of bisphenol A and
647 triclosan among pregnant women in the MIREC cohort. *Environ. Health Perspect*
648 **123**, 277-284 (2015).
649 47. Yang, H., *et al.* A common antimicrobial additive increases colonic inflammation
650 and colitis-associated colon tumorigenesis in mice. *Sci Transl Med* **10**(2018).
651 48. Zhang, J., *et al.* Microbial enzymes induce colitis by reactivating triclosan in the
652 mouse gastrointestinal tract. *Nat Commun* **13**, 136 (2022).
653 49. Fujii, M., *et al.* A murine model for non-alcoholic steatohepatitis showing evidence
654 of association between diabetes and hepatocellular carcinoma. *Med. Mol.*
655 *Morphol* **46**, 141-152 (2013).
656 50. Kim, J.Y., *et al.* ER Stress Drives Lipogenesis and Steatohepatitis via Caspase-
657 2 Activation of S1P. *Cell* **175**, 133-145.e115 (2018).
658 51. Ma, H.Y., *et al.* IL-17 signaling in steatotic hepatocytes and macrophages
659 promotes hepatocellular carcinoma in alcohol-related liver disease. *J Hepatol* **72**,
660 946-959 (2020).
661 52. Oyadomari, S., Harding, H.P., Zhang, Y., Oyadomari, M. & Ron, D.
662 Dephosphorylation of Translation Initiation Factor 2α Enhances Glucose
663 Tolerance and Attenuates Hepatosteatosis in Mice. *Cell Metabolism* **7**, 520-532
664 (2008).

665 53. Pawlak, M., Lefebvre, P. & Staels, B. Molecular mechanism of PPARα action and
666 its impact on lipid metabolism, inflammation and fibrosis in non-alcoholic fatty
667 liver disease. *J Hepatol* **62**, 720-733 (2015).
668 54. Taniguchi, K.*, et al.* A gp130-Src-YAP module links inflammation to epithelial
669 regeneration. *Nature* **519**, 57-62 (2015).
670 55. Lagerborg, K.A., Watrous, J.D., Cheng, S. & Jain, M. High-Throughput Measure
671 of Bioactive Lipids Using Non-targeted Mass Spectrometry. *Methods Mol Biol*
672 **1862**, 17-35 (2019).
673 56. Watrous, J.D.*, et al.* Directed Non-targeted Mass Spectrometry and Chemical
674 Networking for Discovery of Eicosanoids and Related Oxylipins. *Cell Chem Biol*
675 **26**, 433-442.e434 (2019).
676 57. Brunt, E.M. Nonalcoholic steatohepatitis: pathologic features and differential
677 diagnosis. *Semin Diagn Pathol* **22**, 330-338 (2005).
678 58. Dobin, A.*, et al.* STAR: ultrafast universal RNA-seq aligner. *Bioinformatics* **29**,
679 15-21 (2013).
680 59. Bligh, E.G. & Dyer, W.J. A rapid method of total lipid extraction and purification.
681 *Can J Biochem Physiol* **37**, 911-917 (1959).

682

683

METHODS

Mice and treatment options

Breeding pairs of C57/B6 and *Pparα*-null (*Pparα*$^{-/-}$) mice were obtained from Jackson Laboratory (Bar Harbor, ME). ATF4 liver conditional knockout mice (*Atf4*$^{\Delta Hep}$) and control (*Atf4*$^{F/F}$) were obtained from Dr. Christopher M. Adams from the University of Iowa. The intestinal epithelial cell (IEC)-specific expression of the constitutively active gp130 variant (*gp130*^{Act}) mice was produced previously[54]. All animals were housed at the University of California San Diego (UCSD) Animal Care Facility and received food and water ad libitum.

Due to the tendency for TCS to accumulate in many animals and plants that are consumed by humans, we administer TCS in the chow [21]. Breeding pairs of all mice strains (6 weeks old) were fed with a chow diet containing 0.012% TCS (Sigma-Aldrich, 72779) dissolved in vehicle (2ml DMSO + 10ml water) or vehicle alone. The females received TCS in the chow during pregnancy and lactational period (until neonates complete 21 days old). Neonatal mice remained with the breeding pairs for 21 days before being sacrificed, and serum, liver and intestines were collected for analysis. Treatment with TCS did not affect female body weight. For obeticholic acid (OCA, MedChemExpress, HY-12222) experiments, C57/BL6 neonates breastfed TCS were treated with 100 mg/kg of vehicle or OCA (100 mg/kg per day) by oral gavage (p.o.) from day 16 to day 20. The mice were euthanized when they were 21-days old and tissues were collected for further analysis. For all experiments we used only male neonatal mice from at least two independent litters of each treatment group.

The protocols for mice handling and procedures were approved by the UCSD Animal Care and Use Committee (IACUC), and these protocols were conducted in accordance with federal regulations. Animal Protocol S99100 was approved by the UCSD Institutional Animal Care and Use Committee.

Triclosan measurements on milk and serum

We analyzed TCS in the breastmilk of 14-day old neonates. TCS in the serum was analyzed at 21 days. All solvents used for sample preparation and metabolomic analysis were LC/MS grade. Methanol, acetonitrile, water, and isopropanol were purchased from Honeywell International Inc. Ethanol and acetic acid were purchased from Sigma-Aldrich.

All pipetting instruments and consumables were purchased from Eppendorf. LCMS amber autosampler vials and tri-layer vial caps were purchased from Agilent Technologies and 300 µL glass inserts were purchased from Wheaton. Kinetex C18 1.8 mm (100 x 2.1 mm) UPLC columns were purchased from Phenomenex Inc. UPLC BEH RP-18 guard columns were purchased from Waters Inc. Pooled human plasma was obtained from Bioreclamation IVT. Isotopically labeled (13C12) labeled triclosan standard was purchased from Cambridge Isotopes (P/N CLM-6779-1.2).

To each sample, 20 µL of serum and milk was transferred to a clean 1.5 mL microfuge tube. To each sample 80 µL of ethanol extraction solvent containing 250 nM of 13C labeled triclosan was added. Samples were then vortexed at 2000 rpm for 5 minutes at 4 °C to allow for protein precipitation followed by centrifugation at 14,000 rpm for 5 minutes at 4 °C. For each sample, 75 µL of supernatant was transferred to an amber glass HPLC vial (P/N 92-5182-0716) containing a Wheaton 300 µL (P/N 11-0000-100) glass insert. Samples were stored at 4 °C in a Thermo Scientific Vanquish UHPLC autosampler until analysis by LC-MS/MS.

LC-MS/MS Data Acquisition was performed as previously described[55,56]. In brief, 20 µL of sample was injected onto a Phenomenex Kinetex C18 reverse phase column and compounds were eluted with a constant flow rate of 0.375 mL/min using the following gradient: 0-0.25, 99%-99% A, 0.25-5 min, 99%-45% A, 5-5.5 min, 55%-1% A, 5.5-7.5 min,1%A, where mobile phase A is 70:30:0.1 water: acetonitrile: acetic acid and mobile phase B is 50:50:0.02 acetonitrile: isopropanol: acetic acid. Compounds were detected

using a Thermo Scientific QExactive Orbitrap mass spectrometer equipped with a heated electrospray ionization (HESI) source operating in negative ion mode with the following source parameters: sheath gas flow of 40 units, aux gas flow of 15 units, sweep gas flow of 2 units, spray voltage of -3.5 kV, capillary temperature of 265 °C, aux gas temp of 350 °C, S-lens RF at 45. Data was collected using an MS1 scan event followed by 4 DDA scan events using an isolation window of 1.0 m/z and a normalized collision energy of 35 arbitrary units. For MS1 scan events, scan range of m/z 225-650, mass resolution of 17.5k, AGC of 1e6 and inject time of 50 ms was used. For tandem MS acquisition, mass resolution of 17.5 k, AGC 5e5 and inject time of 80 ms was used. TCS was identified by matching accurate mass, retention time and MS/MS fragmentation pattern with commercial standard and quantified using the isotopically labeled internal standard. Data was collected using Thermo Xcalibur software (version 4.1.31.9) and analyzed using Thermo QualBrowser (version 4.1.31.9) as well as MZmine 2.36.

Histology and immunohistochemical procedures

To analyze liver and small intestine (jejunum) morphology, tissue samples were fixed in 10% buffered formalin phosphate (Fisher Chemicals) for analysis at the UCSD Histology Core. Samples were embedded in paraffin, sliced into 5 µm sections and stained with H&E (hematoxylin and eosin). A semi-quantitative summary of the assessment scores for NAFLD histopathology's were performed[57]. For detection of lipid accumulation, frozen liver samples were embedded in Tissue-Tek optimum cutting temperature (OCT) compound, frozen at dry ice, stored in -80ºC and then sliced to 5 µm sections and stained with Oil Red O (ORO) and counterstained with hematoxylin as previously described[6]. For detection of fibrosis, paraffin-embedded sections were stained with Sirius Red as previously described[22,23]. Representative images were captured on an upright light/fluorescent microscope (Zeiss) equipped with AxioCam camera.

For the staining of F4/80 (ThermoFisher, 41-4801-82) and Ki-67 (GeneTex, GTX16667), paraffin liver sections were prepared in the Histology Core (University of California, San Diego). Formalin-fixed, paraffin- embedded liver slides were deparaffinized and rehydrated, using xylene followed by alcohol and PBS washings. Antigen retrieval of tissue slides and the immunohistochemical staining with a primary antibody, secondary biotinylated antibody, and streptavidin-HRP (Pharmingen) were achieved as described previously[22]. Ki-67-positive cells were counted on five fields of four different mice of each group of 200× magnification per slide.

Detection of apoptotic cells in tissue sections was performed by the TUNEL assay with the In-Situ Cell Death Detection Kit (TMR red, Roche), according to the protocol described previously[22]. TUNEL-positive cells were counted on five fields of four different mice of each group of 200× magnification per slide. The quantification of F4/80 staining and Sirius Red was performed in Image J software.

Reverse Transcription Quantitative-PCR

Tissue samples were homogenized in 1mL TRIzol Reagent (Invitrogen, Waltham, MA) according to manufacturer's instructions and total RNA was extracted. Using iScript Reverse Transcriptase (Bio-Rad Laboratories, Hercules, CA), 1 µg of total RNA was used for the generation of cDNA in a total volume of 12 µL as outlined by the manufacturer. Following cDNA synthesis, quantitative PCR was carried out on a CFX96 qPCR system (BioRad) by using SsoAdvanced SYBR Green Supermix (BioRad). Primers sequences are provided in Supplementary Table S2.

RNA Sequencing Analysis

For RNA-seq studies, each RNA sample consisted of RNA from 3 mice, and 3 RNA samples (a total of 9 mice) per group were analyzed as previously performed in our laboratory. The sequencing library was prepared using the Illumina TruSeq RNA Sample

Prep Kit (FC-122-1001; Illumina, San Diego, CA) with 1 ug of total RNA. The sequencing was performed on an NovaSeq 6000 sequencer in the IGM Genomics Center at UCSD. RNA sequencing data analysis was performed by Dr Kristen Jepsen (UCSD). Image deconvolution, quality value calculation, and the mapping of exon reads and exon junctions were performed at the UCSD sequencing core. Base calling was performed using bcl2fastq (v2.17.1.14; Illumina). RNA sequencing reads were aligned Q20 to the mice genome (mm10) with STAR (v2.2.0c)[58] with default parameters, only uniquely alienable reads were used for downstream analysis. Gene expression values were calculated using HOMER by quantifying strand-specific reads across annotated gene exons (RefSeq) and reported as fragments per kilobase of exon per million mapped reads. Sequencing reads were aligned to the Mus musculus (UCSC mm10) genome. Heatmaps were drawn using GraphPad Prism 9.1.0.

Western blot analysis

For whole tissue analyses, minced liver tissue (0.1 mg) was homogenized in 0.4 mL 1 X RIPA lysis buffer (EMD Millipore, Billerica, MA) supplemented with protease inhibitor cocktail (Sigma-Aldrich). After homogenization, the samples were centrifuged at 15,000 x g for 20 min at 4ºC and the supernatants transfer to a new tube and kept at -80ºC until analysis.

Western blots were performed by using NuPAGE 4–12% BisTris-polyacrylamide gels (Invitrogen) with the protocols described by the manufacturer. Protein (30 µg) was electrophoresed at 170 V for 50 min and transferred at 20 V for 2 hours to PVDF membranes (EMD Millipore). Membranes were blocked with 5% non-fat milk at room temperature for 1 hour and incubated with primary antibodies (see reagents), at 4 °C overnight. Membranes were washed and exposed to HRP-conjugated secondary antibodies (anti-mice IgG, anti-rabbit IgG or anti-rat IgG) for 1 hour at room temperature. Protein was detected by the ECL Plus Western blotting detection system (BioRad) and

was visualized by the BioRad Chemidoc Touch Imaging System. Antibodies used for Western Blotting were: GAPDH (Santa Cruz, sc-32233), β-catenin (Santa Cruz, sc-7963), claudin-1 (Santa Cruz, sc-166338), AMPKα1/2 (Santa Cruz, sc-25792), CYP7A1 (Abcam, ab-65596), SCD1 (Santa Cruz, sc-14720), phospho-AMPK (Cell Signaling, CS2535), phospho-eIF2α (Cell Signaling, CS3597), ATF4 (Cell Signaling, CS11815), IL-1β (Cell Signaling, CS12426), cleaved caspase 3 (Cell Signaling, CS9661), FASN (Cell Signaling, CS3180), FOXO1 (Cell Signaling, CS2880), NQO-1 (Cell Signaling, CS62262), cytochrome C (Cell Signaling, CS11940), caspase-9 (Cell Signaling, CS9508S), phospho-β-Catenin (Cell Signaling, CS5651), LGR5 (Abclonal, A10545), SGK1 (Abclonal, A3936). The secondary antibodies anti-mice IgG horseradish peroxidase (HRP) conjugated antibody and anti-rabbit IgG HRP conjugated antibodies were obtained from Cell Signaling Technology, Inc. (Danvers, MA). All primary antibodies were diluted 1:1,000 and secondary antibodies were diluted 1:3,000.

Primary hepatocytes culture and PERK-targeted small interfering RNA (*siRNA*) Regulation

Primary hepatocytes were isolated from 4-week-old C57/B6 mice. Mice were anesthetized and the portal vein was cannulated and perfused with Hanks' balanced salt solution (without Mg^{2+} or Ca^{2+}) followed by perfusion with Hanks' balanced salt solution with Mg^{2+} and Ca^{2+} containing 0.1 mg/mL of Liberase (Roche Applied Science). Following the removal of the liver, the resulting hepatocytes were filtered through a sterile 70-μm filter. The hepatocytes were than cultured in 12-well collagen-treated plates with Dulbecco's modified Eagle's medium (DMEM) medium containing 10% fetal bovine serum (FBS) and penicillin/streptomycin for 6 hours. After changing the medium, the hepatocytes were exposed to TCS at 30 μM with DMEM medium supplemented with 25Mm HEPES, 40ng/mL Dexamethasone, 1x Insulin-transferrin-selenium and

844 penicillin/streptomycin. After 72 hours, hepatocytes were collected for Q-RT-PCR and
845 WB.

846 siRNA specific for mouse PERK (Santa Cruz, sc-36214) and control (Santa Cruz,
847 sc-37007) were purchased at Santa Cruz Biotechnology. Four hours after primary
848 hepatocytes were isolated from 4- to 6- week-old C57/B6 mice, cells were transfected in
849 the presence of 10 nM of either siRNA or control RNA with Lipofectamine RNAiMAX
850 reagent (Invitrogen) in a final volume of 0.5 mL of OPTI-MEM. After 24 hours medium
851 was changed with fresh medium supplemented with 25Mm HEPES, 40ng/mL
852 dexamethasone, 1x insulin-transferrin-selenium and penicillin/streptomycin, containing
853 TCS or DMSO. Lipofectamine and siRNA were kept until the end of the experiment.
854 Fourth-eight hours later, cells were used for RNA and protein extraction. Q-RT-PCR were
855 carried out to examine gene expression levels and WB.

856

857 **Triglyceride and FGF21 ELISA**

858 FGF21 and triglyceride serum levels were measured using FGF-21 Quantikine
859 enzyme-linked immunosorbent assay kit (R&D System), triglyceride colorimetric assay
860 kit (Cayman Chemicals), respectively. Lipid contents were extracted by using Bligh and
861 Dyer method[59] for analysis in liver tissue using the same ELISA kits previously
862 mentioned.

863

864 **Statistical analyses**

865 Data are represented as mean ± SEM. Statistical differences were determined by
866 Student's t test (two groups) or one-way ANOVA (more than 2 groups). *P* values <0.05
867 were considered statistically significant, and statistically significant differences are
868 indicated with **P*<0.5; ***P*<0.01; ****P*<0.001. Statistical analyses were performed using
869 GraphPad 9.1.0 (San Diego, CA).

870

Data Availability

The data reported in this paper have been deposited in the Gene Expression Omnibus (GEO) database with the accession code GSE200705.

SUPPLEMENTARY DATA

Lactational delivery of Triclosan promotes non-alcoholic fatty liver disease in newborn mice

André A. Weber[1], Xiaojing Yang[1], Elvira Mennillo[1], Jeffrey Ding[2], Jeramie D. Watrous[2], Mohit Jain[2], Shujuan Chen[1], Michael Karin[3] Robert H. Tukey[1,*].

Short Title: *Triclosan drives neonatal NAFLD*

[1]Laboratory of Environmental Toxicology, Department of Pharmacology, University of California, San Diego, La Jolla, CA 92093, USA.

[2]Departments of Medicine and Pharmacology, University of California, San Diego, La Jolla, CA 92093, USA.

[3]Laboratory of Gene Regulation and Signal Transduction, Department of Pharmacology, University of California, San Diego, La Jolla, CA 92093.

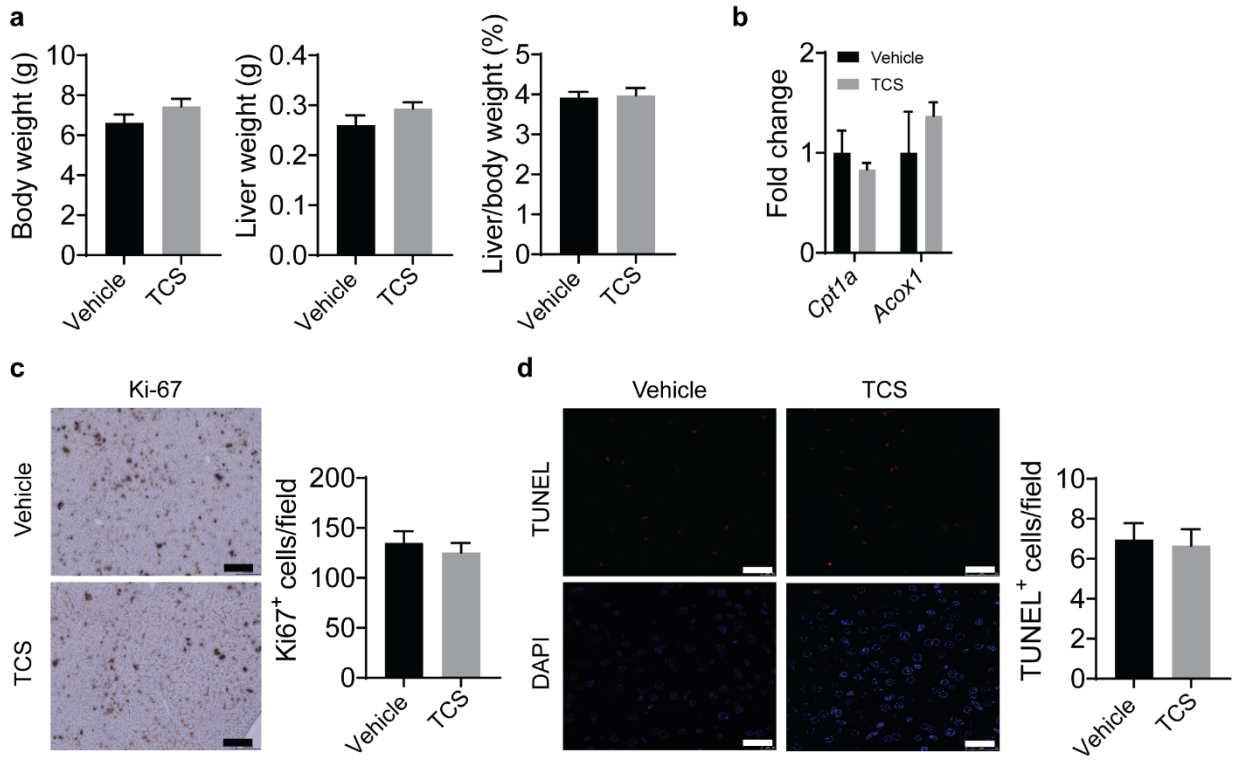

Figure S1. **TCS has no effect on body and liver weight and hepatic proliferation and cell death.** WT mice breastfed with vehicle or TCS for 21-days-old. **a**, Body weight, liver weight and Liver/Body Weight ratio (%) (n=5-6 mice per group). **b.** Expression of genes associated with fatty acid oxidation *Cpt1a* and *Acox1*(n=3 mice per group). **c**, Hepatocyte's proliferation was determined by Ki-67 immunostaining and quantitation of positive cells (n=4 mice per group). **d**, Liver cell apoptosis was determined by TUNEL staining and quantitation of positive cells (n=4 mice per group). a-d show mean ± S.E., determined by two-tailed Student`s test.

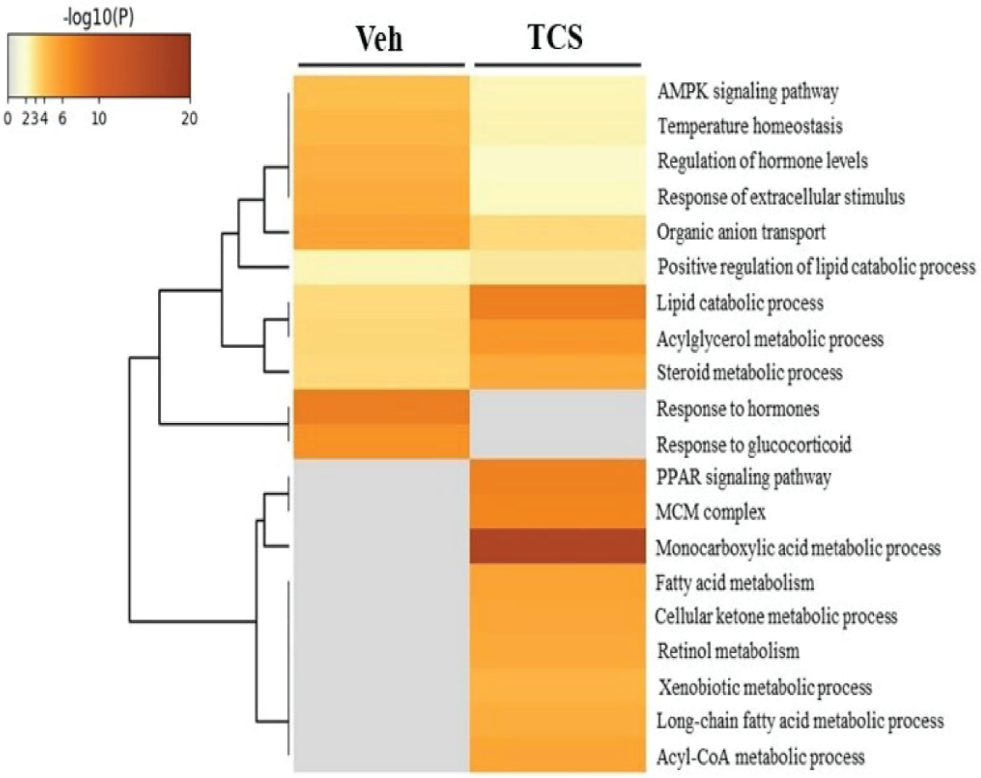

Figure S2. TCS-induced alterations in the liver transcriptome. WT mice breastfed with vehicle or TCS for 21-days-old. Heatmap depicting expression of HCC-related genes in liver tissue of neonatal mice treated with vehicle or TCS (n=3 mice per group). All genes showed in this figure had a *p*-adjusted value above 0.05, showing no differences between groups.

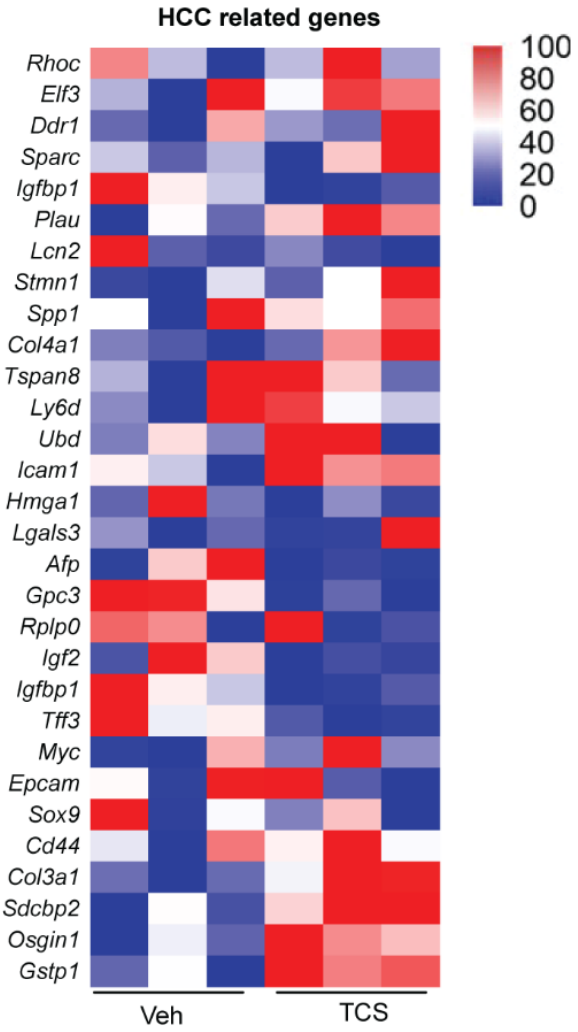

Figure S3. TCS has little effect on HCC-related genes expression. WT mice breastfed with vehicle or TCS for 21-days-old. Heatmap depicting expression of HCC-related genes in liver tissue of neonatal mice treated with vehicle or TCS (n=3 mice per group). All genes showed in this figure had a *p*-adjusted value above 0.05, showing no differences between groups.

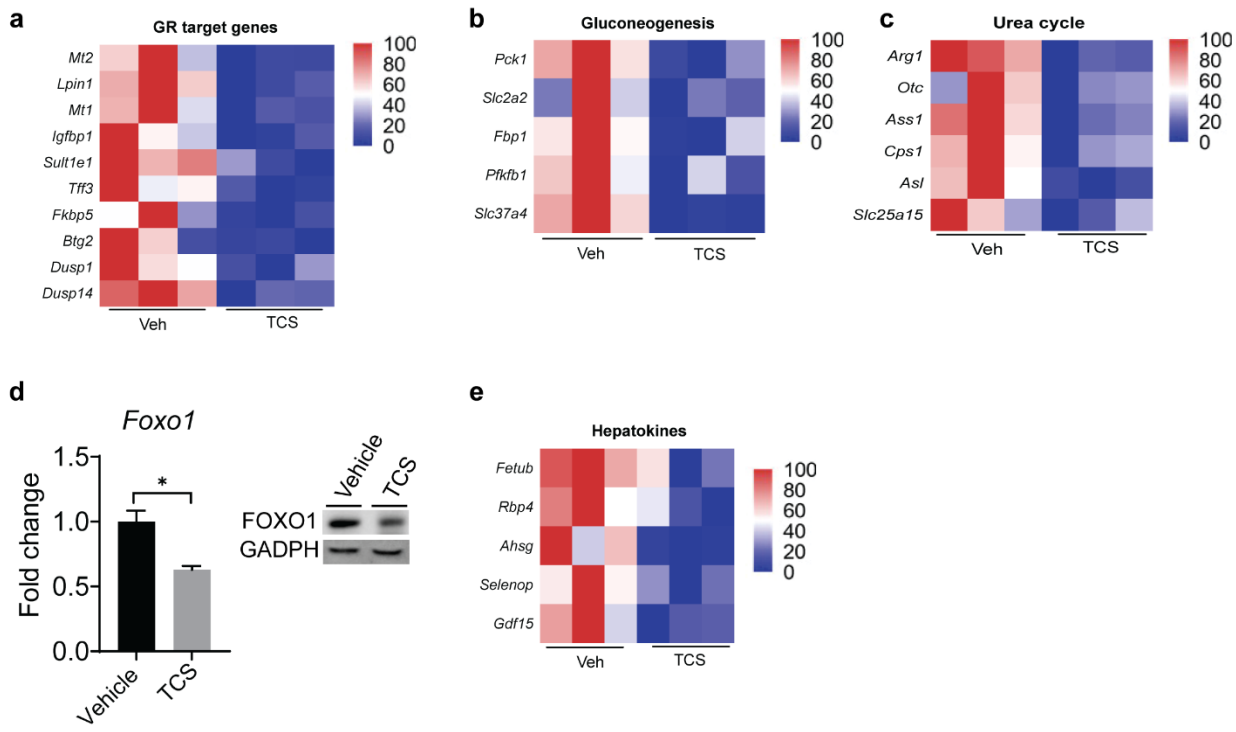

Figure S4. TCS downregulates glucocorticoid receptor and downstream pathways. WT mice breastfed with vehicle or TCS for 21-days-old. **a-c** Heatmaps showing differential expression of genes associated with glucocorticoid receptor (GR) signaling (**a**), and genes associated with downstream GR pathways, gluconeogenesis (**b**) and urea cycle (**c**). **d**, gene expression and representative IB image of FOXO1 in liver (n=3 per group). **e**, Heatmap showing differential expression of hepatokines in liver (n=3 per group). **d** show mean ± S.E., determined by two-tailed Student`s test; **P*<0.05. All genes used are significant and p adjusted value below the cut-off level of 0.05.

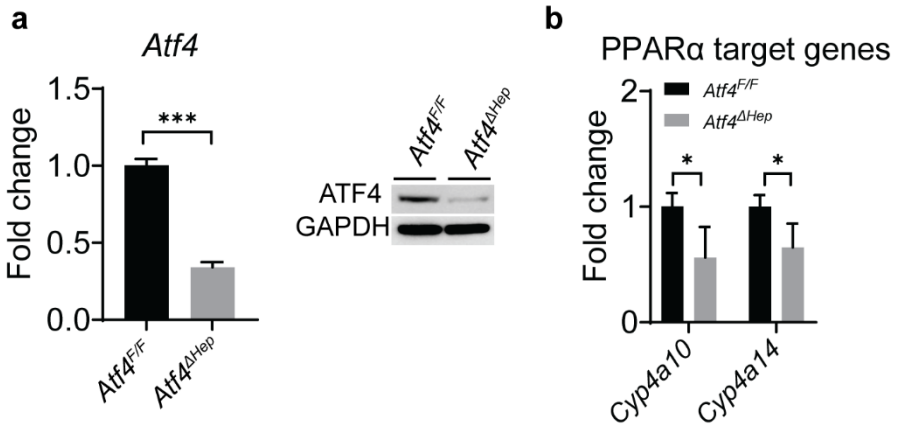

Figure S5. Downstream **PPARα target genes are downregulated in *Atf4*$^{\Delta Hep}$ mice treated with TCS.** *Atf4*$^{F/F}$ and *Atf4*$^{\Delta Hep}$ mice breastfed with TCS milk 21-days-old. **a**, Hepatic expression of ATF4 gene in both *Atf4*$^{F/F}$ and *Atf4*$^{\blacktriangle Hep}$ livers and IB of ATF4 (n=6 mice per group). **b**, Hepatic expression of downstream PPARα target genes in *Atf4*$^{F/F}$ and *Atf4*$^{\blacktriangle Hep}$ (n=3-5 mice per group). **a, b** show mean ± S.E., determined by two-tailed Student`s test; *P<0.05, ***P<0.001.

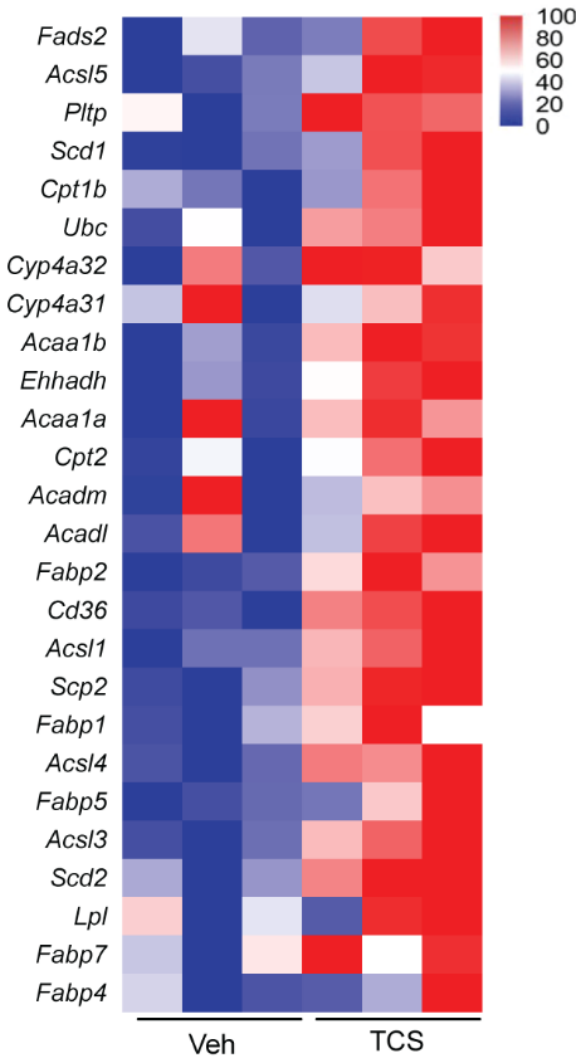

Figure S6. TCS has strong effect on PPARα target genes. WT mice breastfed with vehicle or TCS for 21-days-old. Heatmap depicting expression of downstream PPARα target genes in liver tissue of neonatal mice treated with vehicle or TCS (n=3 mice per group). All genes showed in this figure had a p-adjusted value above 0.05, showing no differences between groups.

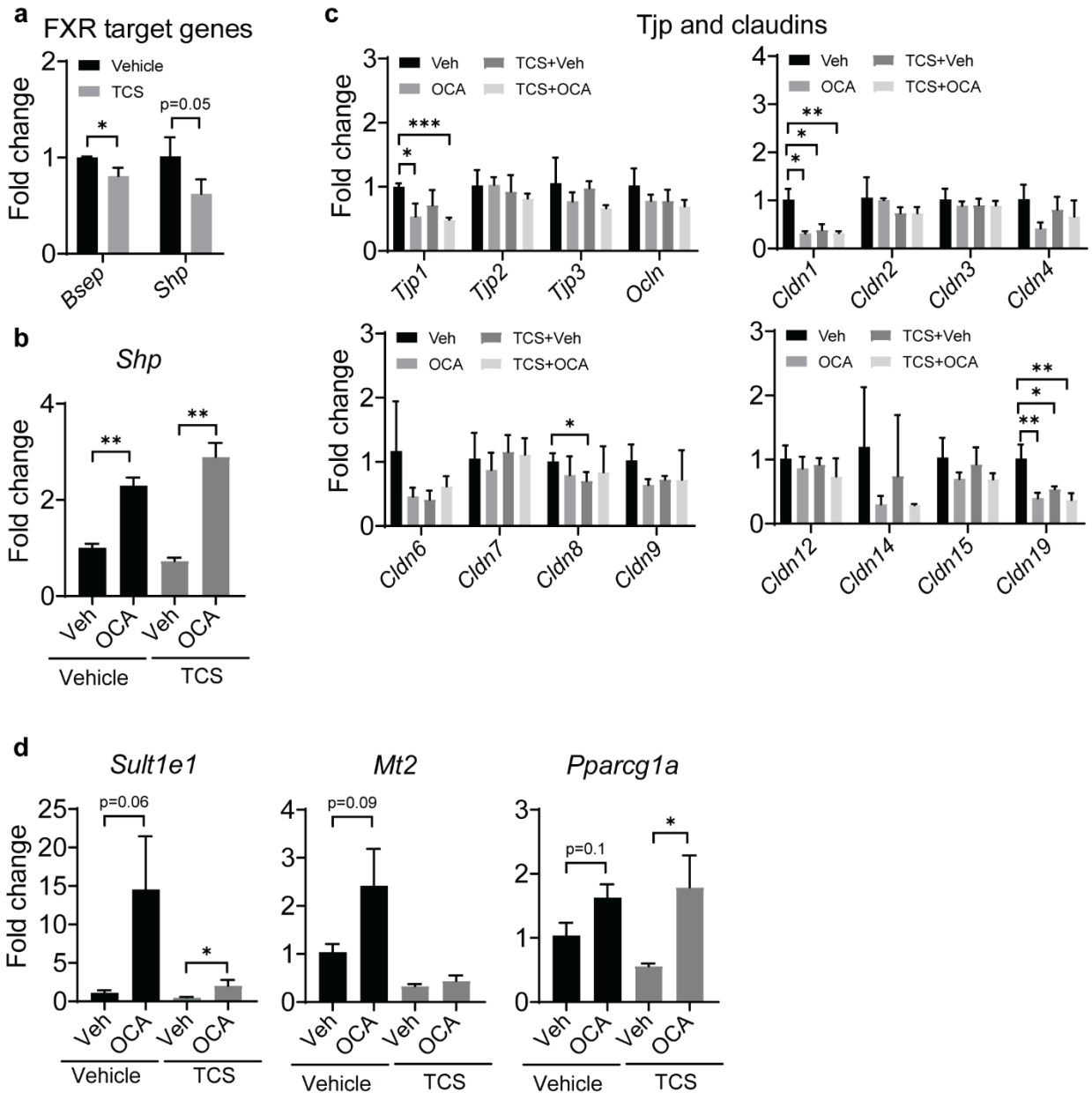

Figure S7. OCA has no effect in intestinal barrier genes but increases GR response in liver in the absence of TCS. WT neonatal mice breastfed with vehicle or TCS milk for 21 days and treated with vehicle or OCA. **a**, Hepatic expression of genes associated with FXR (n=3 mice per group). **b**, Intestinal expression of *Shp* (n=3 mice per group). **c**, Intestinal expression of TJPs, occludin and claudins (n=3 mice per group). **d**, Hepatic expression GR related genes (n=4 mice per group). **a-d** show mean ± S.E., determined by two-tailed Student`s test; *P<0.05, **P<0.01, ***P<0.001.

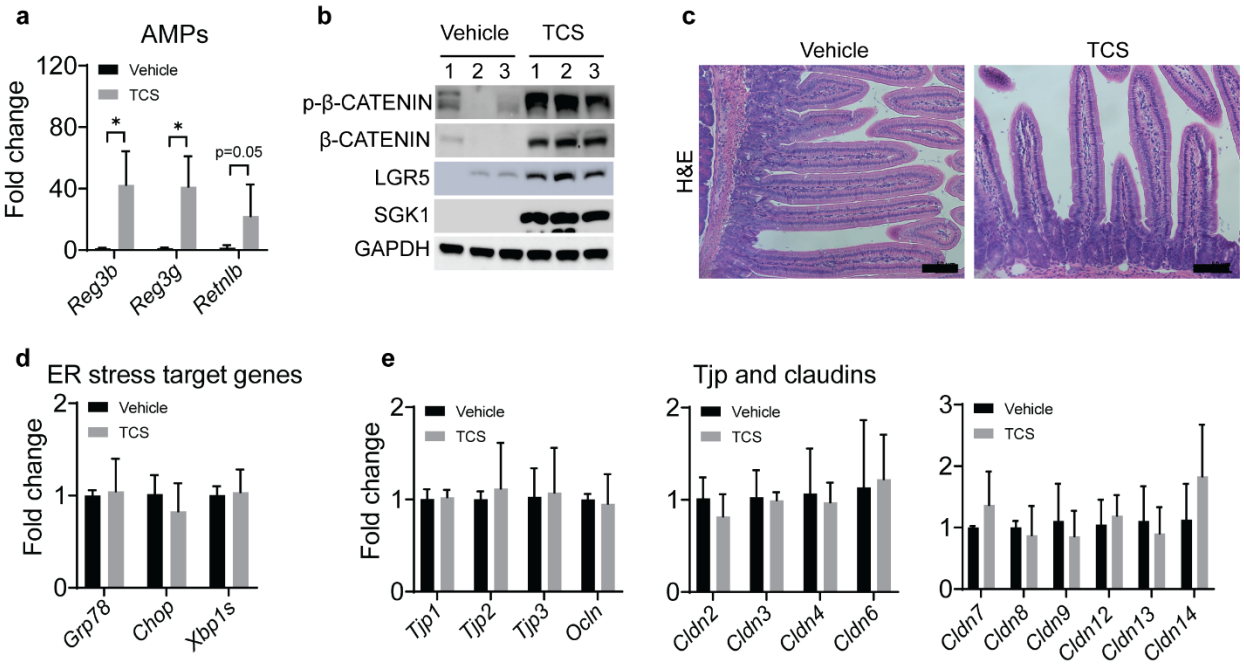

Figure S8. TCS treatment upregulates AMPs and β-catenin pathway in intestines. WT neonatal mice breastfed with vehicle or TCS milk for 21 days. **a**, Intestinal expression of *Reg3b*, *Reg3g* and *Retnlb* (n=3-4 mice per group). **b**, Intestinal IB of total and phosphorylated β-catenin and LGR5 and SGK1 (n=3 mice per group). **c**, Jejunum histological sections were stained with H&E (n=3 per group), Scale bars=50μm. **d,** Intestinal expression of genes associated with ER stress (n=3 mice per group). **e**. Intestinal TJP and claudins genes (n=3 mice per group). **a**, **d** and **e** show mean ± S.E., determined by two-tailed Student`s test; *P<0.05.

Table

Table S1. NAFLD semi-quantitative score in neonatal mice breastfed with TCS.

Histopathology	Vehicle	TCS
Steatosis	0	1
Inflammation	0	1
Fibrosis	0	1
Balloning	0	0
Necrosis	0	0
Total score	**0**	**3**

Table S2. Primer sequences used for Reverse Transcription Quantitative-PCR (RT-qPCR).

Gene name	Forward (5' - 3')	Reverse (5' - 3')
Acaca	TTCCACGTAGGAGGAGCTTCC	CCTCCGGTGCCTTCTCATTAC
Acly	CTGTGCCACCATGTTCTCCTC	AGGCCTGGTTCTTGGCTACTG
Atf4	TTGTCCGTTACAGCAACACTG	GCAGCAGCACCAGGCTCT
Bsep	AAGGACAGCCACACCAACTC	CCAGAACATGACAAACGGAA
Ccne1	TTGCAAGACCCAGATGAAGA	TCCACGCATGCTGAATTATC
Cldn1	ATCACCTTCGGGAGCTCAGGT	TGATGGGGGTCAAGGGGTCAT
Cldn2	ATGCCTTCTTGAGCCTGCTT	CAGTGTCTCTGGCAAGCTGA
Cldn3	CGTACCGTCACCACTACCAG	CAGCCTAGCAAGCAGACTGT
Cldn4	CCATGGAACCCTTCCGTTGA	ACCCGTCCATCCACTCTACA
Cldn6	CCCTTGGTGGCTGATGCTCAA	AGGTGGAGCTTGGACTCAGGT
Cldn7	TGTACCTACCTGGTCCTGGG	TCTCAGAAAAGACGGGACGC
Cldn8	GGAATGCCAATCCATCACGC	CTCTTTTATCCCCAGGCCCC
Cldn9	AAGTGGTATGGGAGGGGCTGT	CGCAGGTGGAAGCTTCTGGAA
Cldn12	TGTGTGCAGATGTGCTCCTGT	GCAGGAGGGCTTGAGCTGTAT
Cldn14	CTAACCAGAGGGCATGTGTGC	AGTCCCATCCACCTTGATGCT
Cldn15	GGTGGCTATCTCGTGGTACG	GCACTCCAGCCCAAGTAGAG
Cldn19	GGAATTCTTCAACCCCAGCAC	ATAGGGCTGTGGGATGCTGTT
Chop	CCACCACACCTGAAAGCAGAA	AGGTGAAAGGCAGGGACTCA
Ctgf	CAGACTGGAGAAGCAGAGCC	GCTTGGCGATTTTAGGTGTC
Cyclophiline	CAGACGCCACTGTCGCTT	TGTCTTTGGAACTTTGTCTGC
Cyp4a14	ACCCCTCTAGATTTGCACCA	AGCAAACTGTTTCCCAATGC
Cyp4a10	CACACCCTGATCACCAACAG	TCCTTGATGCACATTGTGGT
Edem1	CTACCTGCGAAGAGGCCG	GTTCATGAGCTGCCCACTGA
Ehhadh	CTATGATCCGCCTCTGCAA	TGGCTCTAACCGTATGGTCC
Fabp1	TGCAGAGCCAGGAGAACTTT	GATTTCTGACACCCCCTTGA
Fgf21	CTCCAGCAGTTCTCTGA	CCTGGGTGTCAAAGCCTCTA
Fasn	AGAAGAGCCATGGAGGAGGTG	ATGTCCACACCACCAATGAGG
Grp78	TTCAGCCAATTATCAGCAAACTCT	TTTTCTGATGTATCCTCTTCACCAGT
Mlxipl	CGGATACGGACTTGGAGGATC	GAAGTGTCCGCTGTGGATGAC
Mt2	TTGCGCTCGACCCAATACTC	CATTGTTTGCATTTGCAGGCG
Ocln	TCCGGATCCTGTCTATGCTCA	ATAGCCACCTCCGTAGCCAAA
Perk	TCATCCAGCCTTAGCAAACC	ATGCTTTCACGGTCTTGGTC
Pparcg1a	AAGTGGTGTAGCGACCAATCG	AATGAGGGCAATCCGTCTTCA
Reg3b	CCCAAGGGCTCCCAGGCTTA	GAGGTGTCCTCCAGGCCTCT

Reg3g	TGGCGCTGAAGCTTCCTTCC	TCATAGCCCAGTGTCGGGTCA
Retnlb	CCATTTCCTGAGCTTTCTGG	AGCACATCCAGTGACAACCA
Scd1	GCTCTACACCTGCCTCTTCG	CAGCCGAGCCTTGTAAGTTC
Shp	CACGATCCTCTTCAACCCAG	AGACTTCACACAGTGCCCA
Srebf1	GGCTCTGGAACAGACACTGG	TGGTTGTTGATGAGCTGGAG
Sult1e1	AAACTCACCTGCCACCCAAG	TTGGCGTTCCGGCAAAGATA
Xbp1s	CTGAGTCCGAATCAGGTGCAG	GTCCATGGGAAGATGTTCTGG
Tjp1	GAAACTCTGCTGAGCCCCCTA	GTTTTAGGGTCACCCGACGAG
Tjp2	CGAAGCAGTCTGGGTCTCTGA	CCGGCTCCTCTAGCTCATTGT
Tjp3	ATGGTATGCCATTTCGGAACC	CCGGGTACAACGTGTCCACTA